THE JOURNAL OF BIOLOGICAL CHEMISTRY
Vol. 276, No. 41, Issue of October 12, pp. 38121–38138, 2001

Printed in U.S.A.

Caveolin-1 Null Mice Are Viable but Show Evidence of Hyperproliferative and Vascular Abnormalities*

Received for publication, June 12, 2001, and in revised form, July 13, 2001
Published, JBC Papers in Press, July 16, 2001, DOI 10.1074/jbc.M105408200

Babak Razani‡§, Jeffery A. Engelman‡, Xiao Bo Wang‡, William Schubert‡, Xiao Lan Zhang‡, Carolyn B. Marks¶, Frank Macaluso¶, Robert G. Russell‖, Maomi Li, Richard G. Pestell‡‡***, Dolores Di Vizio‡‡, Harry Hou, Jr.§§, Burkhard Kneitz§§, Guy Lagaud¶¶, George J. Christ¶¶, Winfried Edelmann§§, and Michael P. Lisanti‡‖‖**

*From the ‡Department of Molecular Pharmacology and The Albert Einstein Cancer Center, the ¶Analytical Imaging Facility, the ‖Department of Pathology and Institute for Animal Studies, the **Department of Pathology, ‡‡Departments of Developmental and Molecular Biology and Medicine, and The Albert Einstein Cancer Center, the §§Department of Cell Biology and The Albert Einstein Cancer Center, the ¶¶Departments of Urology, Physiology, and Biophysics, Institute for Smooth Muscle Biology, The Albert Einstein College of Medicine, Bronx, New York 10461*

Caveolin-1 is the principal structural protein of caveolae membranes in fibroblasts and endothelia. Recently, we have shown that the human *CAV-1* gene is localized to a suspected tumor suppressor locus, and mutations in Cav-1 have been implicated in human cancer. Here, we created a caveolin-1 null (CAV-1 −/−) mouse model, using standard homologous recombination techniques, to assess the role of caveolin-1 in caveolae biogenesis, endocytosis, cell proliferation, and endothelial nitric-oxide synthase (eNOS) signaling. Surprisingly, Cav-1 null mice are viable. We show that these mice lack caveolin-1 protein expression and plasmalemmal caveolae. In addition, analysis of cultured fibroblasts from Cav-1 null embryos reveals the following: (i) a loss of caveolin-2 protein expression; (ii) defects in the endocytosis of a known caveolar ligand, *i.e.* fluorescein isothiocyanate-albumin; and (iii) a hyperproliferative phenotype. Importantly, these phenotypic changes are reversed by recombinant expression of the caveolin-1 cDNA. Furthermore, examination of the lung parenchyma (an endothelial-rich tissue) shows hypercellularity with thickened alveolar septa and an increase in the number of vascular endothelial growth factor receptor (Flk-1)-positive endothelial cells. As predicted, endothelial cells from Cav-1 null mice lack caveolae membranes. Finally, we examined eNOS signaling by measuring the physiological response of aortic rings to various stimuli. Our results indicate that eNOS activity is up-regulated in Cav-1 null animals, and this activity can be blunted by using a specific NOS inhibitor, nitro-L-arginine methyl ester. These findings are in accordance with previous *in vitro* studies showing that caveolin-1 is an endogenous inhibitor of eNOS. Thus, caveolin-1 expression is required to stabilize the caveolin-2 protein product, to mediate the caveolar endocytosis of specific ligands, to negatively regulate the proliferation of certain cell types, and to provide tonic inhibition of eNOS activity in endothelial cells.

Caveolin was first identified in 1989 by Glenney and colleagues (1, 2) as a major v-Src substrate in Rous sarcoma virus-transformed chicken embryo fibroblasts. Interestingly, this same protein was found to be the primary structural component of caveolae microdomains, 50–100 nm vesicular invaginations of the plasma membrane (3).

Caveolae were morphologically described as early as the 1950s by Yamada (4) and Palade (5). They are curious structures that can be found individually or in clusters at the surfaces of numerous cell types, the best examples of which are adipocytes, endothelial cells, muscle cells, and fibroblasts. Research in the past decade has shown that caveolae are specialized membrane microdomains formed as a result of localized accumulation of cholesterol, glycosphingolipids, and caveolin (6–8). Caveolin, an integral membrane protein that can directly bind cholesterol, most likely plays a major role in the invagination of caveolae from the plasma membrane proper, although our understanding of the mechanisms behind this process remains rudimentary.

Two other members of the caveolin gene family have recently been identified and cloned, caveolin-2 and caveolin-3 (9, 10); as a consequence, caveolin has been re-termed caveolin-1 (Cav-1).[1] Caveolin-2 has the same tissue distribution as and co-localizes with caveolin-1, whereas caveolin-3 is expressed only in cardiac, skeletal, and smooth muscle cells (11, 12).

* The costs of publication of this article were defrayed in part by the payment of page charges. This article must therefore be hereby marked "*advertisement*" in accordance with 18 U.S.C. Section 1734 solely to indicate this fact.This work was supported in part by grants from the National Institutes of Health, the Muscular Dystrophy Association, the American Heart Association, and the Komen Breast Cancer Foundation (to M. P. L.).

§ Supported by a National Institutes of Health (NIH) Medical Scientist Training Grant T32-GM07288.

‖‖ Recipient of a Hirschl/Weil-Caulier Career Scientist Award. To whom correspondence should be addressed: Dept. of Molecular Pharmacology and The Albert Einstein Cancer Center, Albert Einstein College of Medicine, 1300 Morris Park Ave., Bronx, NY 10461. Tel.: 718-430-8828; Fax: 718-430-8830; E-mail: lisanti@aecom.yu.edu.

*** Supported by NIH Grants R01-CA70897, R01-CA86072, and R01-CA75503, the Komen Breast Cancer Foundation, and the Department of Defense. Recipient of a Hirschl/Weil-Caulier Career Scientist Award.

[1] The abbreviations used are: Cav-1, caveolin-1; Cav-2, caveolin-2; Cav-3, caveolin-3; eNOS, endothelial nitric-oxide synthase; FITC, fluorescein isothiocyanate; L-NAME, nitro-L-arginine methyl ester; MAP, mitogen-activated protein; EGF, epidermal growth factor; EGF-R, EGF receptor; VEGF-R, vascular endothelial growth factor receptor; mAb, monoclonal antibody; kb, kilobase pair; bp, base pair; PCR, polymerase chain reaction; MEF, mouse embryonic fibroblast; PAGE, polyacrylamide gel electrophoresis; GFP, green fluorescent protein; PBS, phosphate-buffered saline; BSA, bovine serum albumin; DMEM, Dulbecco's modified Eagle's medium; FBS, fetal bovine serum; PFUs, plaque-forming units; KO, knockout; NO, nitric oxide; NOS, nitric-oxide synthase; PE, phenylephrine; Ach, acetylcholine; pAb, polyclonal antibody; Mes, 4-morpholine-ethanesulfonic acid; ES, embryonic stem; CSD, caveolin-1 scaffolding domain.

Although caveolae function in vesicular and cholesterol trafficking (13, 14), they have also been implicated in signal transduction at the plasma membrane (15, 16). Biochemical and morphological experiments have shown that a variety of lipid-modified signaling molecules are concentrated within these plasma membrane microdomains, such as Src family tyrosine kinases, Ha-Ras, eNOS, and heterotrimeric G-proteins (17–22).

In many ways, caveolin-1 is intricately involved in caveolar functioning. In the years after the discovery that caveolae might serve to compartmentalize signaling molecules and facilitate cross-talk among signaling cascades (the so-called "caveolae signaling hypothesis" (16)), Cav-1 has been found to be a key regulator of some of these proteins. Both *in vitro* and cell culture experiments indicate that Cav-1 can directly interact with and maintain some of these signaling molecules in an inactive conformation (reviewed in Ref. 23). In effect, Cav-1 seems to act as a scaffolding protein, able to negatively regulate the activity of other molecules by binding to and releasing them in a timely fashion.

Research in the past few years has established a recurring theme in this regulation. Many of the proteins that either interact with, transcriptionally repress, or are inhibited by Cav-1 fall under the pro-proliferative, oncogenic, and anti-apoptotic category of molecules. Cav-1 interacts with and negatively regulates the EGF-R, platelet-derived growth factor receptor, and Neu tyrosine kinases (24–26), Ha-Ras (17, 18), c-Src (17), and phosphatidylinositol 3-kinase (27). Conversely, caveolin-1 levels are transcriptionally reduced upon activation of the oncogenes Ha-*ras*, v-*abl*, *myc*, *neu*, the HPV oncogene *E6*, among others (26, 28–30). Therefore, it is not surprising that we and others (26, 29, 31–37) observed undetectable or very low expression levels of Cav-1 in numerous tumor-derived cell lines.

For some time, it has been known that a certain locus (D7S522; 7q31.1) is an aphidicolin-induced fragile site in the human genome (38, 39) and a hot spot for deletions in a variety of human tumors including breast, prostate, colorectal, ovarian, pancreatic, and renal cell carcinomas (38, 40–46). Interestingly, determination of the genomic organization of the human *CAV-1* locus revealed that it maps to 7q31.1, adjacent to the LOH marker D7S522, and as of yet it still remains the closest known gene to this putative tumor suppressor locus (35, 47).

Taken together, the results described above have led many investigators to propose the possibility that Cav-1 is indeed a "tumor suppressor" whose reduction/deletion in cells would provide growth advantages and expedite tumorigenesis. In support of this idea, the only two methods thus far used to abolish Cav-1 expression have arrived at similar conclusions. Antisense-mediated down-regulation of Cav-1 in NIH-3T3 fibroblasts leads to a hyperactivation of the p42/44 MAP kinase pathway and anchorage-independent growth (48). An RNA interference-based ablation of Cav-1 in *Caenorhabditis elegans* leads to progression of the meiotic cell cycle, a phenotype that mirrors that of Ras activation (49).

Furthermore, a recent report indicates that the caveolin-1 gene is mutated in up to 16% of human breast cancer samples examined (50). Recombinant expression of the caveolin-1 cDNA harboring this mutation (P132L) was sufficient to transform NIH 3T3 cells (50). As similar results have been obtained previously using an antisense approach to ablate caveolin-1 expression (48), these results indicate that the caveolin-1 (P132L) mutation may behave in a dominant-negative fashion. Interestingly, an analogous mutation occurs within the caveolin-3 gene (P104L) in patients with a novel form of autosomal dominant limb-girdle muscular dystrophy (LGMD-1C) (51).

In order to gain a better understanding of caveolae and caveolin-1 functioning in a mammalian organism, we used a gene targeting strategy to disrupt the Cav-1 locus in the mouse. In this way, we could observe the role Cav-1 plays in animal physiology (*i.e.* during development and into adult life) as well as molecularly (*i.e.* caveolar biogenesis, its interaction with caveolin-2, and its functional roles in endocytosis, cellular proliferation, and signal transduction). In this study, we describe the generation of mice lacking the *cav-1* gene and determine some of the molecular side effects that result from a deficiency of Cav-1 expression.

Undoubtedly, the generation of viable/fertile Cav-1-deficient mice (and cells derived from these animals) will allow us and others to critically evaluate the many proposed functions of caveolae organelles and the caveolin-1 protein *in vivo*.

EXPERIMENTAL PROCEDURES

Materials—Antibodies and their sources were as follows: anti-caveolin-1 mAb 2297, anti-caveolin-2 mAb 65, and anti-caveolin-3 mAb 26 (10, 11, 52) (gifts of Dr. Roberto Campos-Gonzalez, BD Transduction Laboratories, Inc.); anti-caveolin-1 pAb N-20 (Santa Cruz Biotechnology); anti-p42/44 pAb and phospho-specific anti-p42/44 pAb (New England Biolabs); anti-β-tubulin mAb TUB-2.1 and anti-β-actin mAb AC-15 (Sigma). A variety of other reagents were purchased commercially as follows: cell culture reagents and the LipofectAMINE liposomal transfection reagent were from Life Technologies, Inc.

Construction of the Targeting Vector—Genomic clones containing the murine Cav-1 locus were isolated from a 129/Sv(J1) λ-phage genomic library (53, 54) by using probes corresponding to the murine Cav-1 cDNA. The genomic organization of the locus was determined by subcloning portions of these genomic inserts into the vector pBS-SK$^+$ (Stratagene) and using Southern blotting to determine a detailed restriction map of the region (55). One of the genomic clones (containing the first and second exons of Cav-1) was used to construct the targeting vector. Briefly, a 2.7-kb *Not*I-*Eco*RI fragment that is immediately 5′ to the first exon and a 2.1-kb *Bam*HI-*Bam*HI fragment that is immediately 3′ to the second exon of the *cav-1* gene were used to flank the NEO cassette in the targeting vector pGT-N29 (New England Biolabs) (as shown in Fig. 1).

Screening of Homologously Recombined ES Cells and Generation of Germ Line Chimeras—WW6 ES cells (gift of Dr. Pamela Stanley (56)) were electroporated with the linearized targeting construct (40 μg) and selected with G418 (150 μg/ml of active component, Life Technologies, Inc.) as described previously (57). Homologous recombination in 360 selected ES clones was assessed via Southern blot analysis. Briefly, genomic DNA was digested with *Pst*I or *Xba*I and hybridized with a 1.1-kb *Xba*I-*Sac*I probe; Cav-1+/− clones produced an 8.0-kb wild-type and a 5.5-kb knockout band (*Pst*I digest) or a 10.0-kb wild-type and a 4.0-kb knockout band (*Xba*I digest) (as shown in Fig. 1). Four Cav-1+/− ES clones were microinjected into C57BL/6 blastocysts, and three gave rise to male chimeras with a significant ES cell contribution (as determined by an Agouti coat color). By mating with C57BL/6 females and genotyping of offspring tail DNA via Southern and PCR analysis, germ line transmission was confirmed for two separate clones (Fig. 1). F1 male and female heterozygous animals were interbred to obtain Cav-1-deficient animals. To facilitate the genotyping of all future mice, we also devised a 3-primer PCR-based screening strategy. The wild-type specific forward primer was derived from Cav-1 exon 2 (5′-GTGTATGACGCGCACACCAAG-3′); the knockout-specific forward primer was derived from the neomycin cassette (5′-CTAGTGAGACGTGCTACTTCC-3′), and the common reverse primer was derived from Cav-1 intron 2 (5′-CTTGAGTTCTGTTAGCCCAG-3′). PCR conditions were 95 °C/5 min, 35 cycles of (95 °C/1 min, 56 °C/1 min, 72 °C/1 min 20 s) and then 72 °C/7 min, which resulted in a ~650-bp wild-type band and a ~330-bp knockout band.

Animals were analyzed at 2–4.5 months of age. Experiments were conducted under the direct supervision of the trained veterinarians of the Einstein Animal Institute, and animal protocols were approved by the Animal Use Committee.

Mouse Embryonic Fibroblast (MEF) Culture and Immortalization Protocol—Primary MEFs were obtained from Day 13.5 embryos essentially as described (58). Briefly, embryos were decapitated, thoroughly minced, and trypsinized in 1 ml of 0.05% trypsin, 0.53 mM EDTA (Life Technologies, Inc.) for 20 min at 37 °C. Ten ml of complete medium (Dulbecco's modified Eagle's medium (DMEM) supplemented with 10% fetal bovine serum (FBS), 2 mM glutamine, 100 units/ml penicillin, and

100 μg/ml streptomycin (Life Technologies, Inc.)) was used to inactivate the trypsin and resuspend the dissociated cells. Cells were plated on a 10-cm plate and cultured in a 37 °C, 5% CO_2 incubator. These "passage 1" cells were further propagated using a defined 3T3 passaging protocol (*i.e.* 3×10^5 cells were plated per 60-mm dish every 3 days). For all experiments early passage primary MEFs (<5) were used. To immortalize MEFs, cells were passaged according to the 3T3 protocol continuously until growth rates in culture resumed the rapid rates seen in early passage MEFs (*i.e.* Passage 25 cells and beyond).

Transmission Electron Microscopy—MEFs were fixed with 2.5% glutaraldehyde in 0.1 M cacodylate buffer post-fixed with OsO_4, and stained with uranyl acetate and lead citrate. A cryotome was used to yield sections, and the samples were examined under a JEOL 1200EX transmission electron microscope and photographed at a magnification of × 16,000 (59–61). Caveolae were identified by their characteristic flask shape, size (50–100 nm), and location at or near the plasma membrane (28).

Expression Vectors—The cDNA encoding full-length caveolin-1 was subcloned into pCB7, a mammalian expression vector driven by the cytomegalovirus promoter (62). The cDNAs encoding GFP and GFP-Cav-1 (containing the full-length Cav-1 cDNA C-terminal to GFP) were as described previously (63).

Immunoblot Analysis—Cells were cultured in their respective media and allowed to reach 80–90% confluency. Subsequently, they were washed with PBS and incubated with lysis buffer (10 mM Tris, pH 7.5; 50 mM NaCl; 1% Triton X-100; 60 mM octyl glucoside) containing protease inhibitors (Roche Molecular Biochemicals). Protein concentrations were quantified using the BCA reagent (Pierce), and the volume required for 10 μg of protein was determined. Samples were separated by SDS-PAGE (12.5% acrylamide) and transferred to nitrocellulose. The nitrocellulose membranes were stained with Ponceau S (to visualize protein bands) followed by immunoblot analysis. All subsequent wash buffers contained 10 mM Tris, pH 8.0, 150 mM NaCl, 0.05% Tween 20, which was supplemented with 1% bovine serum albumin (BSA) and 2% nonfat dry milk (Carnation) for the blocking solution and 1% BSA for the antibody diluent. Primary antibodies were used at a 1:500 dilution. Horseradish peroxidase-conjugated secondary antibodies (1:5000 dilution, Pierce) were used to visualize bound primary antibodies with the Supersignal chemiluminescence substrate (Pierce).

Purification of Caveolae-enriched Membrane Fractions—Caveolae-enriched membrane fractions were purified essentially as we described previously (59). 200 mg of lung tissue was placed in 2 ml of MBS (25 mM Mes, pH 6.5, 150 mM NaCl) containing 1% Triton X-100 and solubilized by using quick 10-s bursts of a rotor homogenizer and passing 10 times through a loose fitting Dounce homogenizer. The sample was mixed with an equal volume of 80% sucrose (prepared in MBS lacking Triton X-100), transferred to a 12-ml ultracentrifuge tube, and overlaid with a discontinuous sucrose gradient (4 ml of 30% sucrose, 4 ml of 5% sucrose, both prepared in MBS, lacking detergent). The samples were subjected to centrifugation at 200,000 × *g* (39,000 rpm in a Sorval rotor TH-641) for 16 h. A light scattering band was observed at the 5–30% sucrose interface. Twelve 1-ml fractions were collected, and 50-μl aliquots of each fraction were subjected to SDS-PAGE and immunoblotting.

Immunofluorescence Microscopy—The procedure was performed as we described previously (17). MEFs (either un-transfected or transfected with the caveolin-1 cDNA) were fixed for 30 min in PBS containing 2% paraformaldehyde, rinsed with PBS, and quenched with 50 mM NH_4Cl for 10 min. The cells were then incubated in permeabilization buffer (PBS; 0.2% BSA; 0.1% Triton X-100) for 10 min, washed with PBS, and double-labeled with a 1:400 dilution of anti-caveolin-1 pAb N-20 and 1:200 dilution of anti-caveolin-2 mAb for 60 min. After rinsing with PBS (3 times), secondary antibodies (7.5 μg/ml) ((lissamine-rhodamine-conjugated goat anti-rabbit and fluorescein (FITC)-conjugated goat anti-mouse) antibodies (Jackson ImmunoResearch) were added for a period of 60 min. Cells were washed with PBS (3 times) and slides mounted with Slow-Fade anti-fade reagent (Molecular Probes). A Bio-Rad MR600 confocal fluorescence microscope was used for visualization of bound secondary antibodies.

Rescue of Caveolin-2 Levels in Caveolin-1-deficient MEFs—The construction and characterization of the Cav-1 and GFP Adenoviruses were as we described previously (34). MEF infections were conducted as follows: 10^5 cells were seeded in a series of 35-mm dishes. The desired viral titer (quantified as plaque-forming units (PFUs)) was aliquoted and preincubated with 10^4 molecules of poly-L-lysine per viral particle in PBS for 30 min. Serum-free medium up to 1 ml was added to this solution and placed on the cells for 2 h. Cells were then cultured in regular growth medium (DMEM, 10% FBS) for 48 h and subjected to immunoblot analysis. The lysosomal/proteasomal inhibitor experiments were performed essentially as described (64). Briefly, 1.5×10^5 cells were seeded in a series of 35-mm dishes and treated for the indicated times with vehicle alone (Me_2SO) or with either the proteasomal inhibitors MG-132 (1 μM, Sigma) or MG-115 (1 μM, Sigma) or the lysosomal inhibitors chloroquine (50 μM, Sigma) or NH_4Cl (10 mM). Cells were then lysed and subjected to immunoblot analysis.

Endocytosis Assays—Wild-type and Cav-1 null mouse embryo fibroblasts (MEFs) were plated on 18-mm glass coverslips (Fisher) in 12-well plates. Cells were grown in complete medium (DMEM supplemented with 10% FBS, 2 mM glutamine, 100 units/ml penicillin, and 100 μg/ml streptomycin (Life Technologies, Inc.)). When cells reached ~75–85% confluency, the media was replaced with 1 ml of complete media containing FITC-conjugated albumin (Sigma) at a final concentration of 10 μg/ml. Cells were incubated at 37 °C for 5, 15, and 30 min, washed in PBS, and fixed in 2% paraformaldehyde for 20 min. The cells were washed for 20 min in PBS and mounted on slides with the Prolong anti-fade reagent (Molecular Probes) and imaged with an Olympus IX 70 inverted microscope. Virtually identical experiments were carried out with FITC-conjugated transferrin (10 μg/ml; Sigma).

Caveolin-1 knockout MEFs were grown on 60-mm tissue culture dishes and transiently transfected with the caveolin-1 cDNA in the pCB7 vector using LiopfectAMINE Plus (Life Technologies, Inc.), according to the manufacturer's instructions. The transfected cells were plated on 18-mm coverslips in 12-well plates after 24 h. FITC-albumin uptake was then examined in the transfected cells 36 h after the initial transfection. Cells transfected with caveolin-1 were detected by immunostaining with anti-Cav-1 IgG (N-20; Santa Cruz Biotechnology) and a rhodamine-conjugated secondary antibody.

MEF Proliferation Curves and Cell Cycle Analysis—Proliferation curves were conducted essentially as described previously (65). Briefly, 15×10^3 cells were seeded in a series of twenty 35-mm dishes and cultured under regular growth conditions (DMEM, 10% FBS). Each day, two plates were counted using a hemocytometer, and the medium was changed for the remaining plates. Growth curves were continued for a 10-day time course.

Cell cycle analysis was conducted by Flow Cytometry essentially as described (66). Briefly, 2×10^5 cells were seeded in 60-mm dishes and cultured under regular growth conditions (DMEM, 10% FBS) for 24 h. Cells were trypsinized, washed in PBS, and fixed in 70% ethanol at 4 °C for at least 30 min. Fixed cells were resuspended in PBS containing 0.25 mg/ml RNase A (Sigma) and 10 μg/ml propidium iodide (Sigma) and subjected to univariate cell cycle analysis using a Becton-Dickinson FACScan flow cytometer. The G_0/G_1, S, and G_2/M phases of the cell cycle were quantified with CELLQUEST software.

DNA synthesis in MEFs was directly analyzed by [^{3}H]thymidine incorporation, essentially as described (66). Briefly, 2×10^5 cells were seeded in five 60-mm dishes, allowed to adhere, and cultured overnight under regular growth conditions (DMEM, 10% FBS) supplemented with 1 μCi of [^{3}H]thymidine. Cells were washed with PBS, lysed in 0.3 M NaOH, and fixed with 10% trichloroacetic acid at 4 °C for 30 min. The precipitated material was centrifuged, washed, and resuspended in 200 μl of 0.3 M NaOH, 100 μl of which was quantified using a scintillation counter.

Light and Electron Microscopic Analysis of the Lung—Lung tissue samples were fixed with 2.5% glutaraldehyde in 0.1 M sodium cacodylate buffer, postfixed with 1% osmium tetroxide followed by 1% uranyl acetate, dehydrated through a graded series of ethanol, and embedded in LX112 resin (LADD Research Industries, Burlington VT). Ultrathin sections were cut on a Reichert Ultracut E, stained with uranyl acetate followed by lead citrate, and viewed using a JEOL 1200EX transmission electron microscope at 80 kV. One-μm thick sections were stained with toluidine blue and imaged on a Zeiss Axiophot microscope.

Preparation of Lung Paraffin Sections—Wild-type and Cav-1 null mice were sacrificed and the lungs removed and placed in 10% formalin. The lungs were then inflated by injecting fixative with a syringe directly into the lungs to preserve the alveolar structure. The tissue was fixed for 2 h, washed in PBS for 20 min, and dehydrated through a graded series of ethanol washes. The tissue was then treated with xylene for 40 min all at room temperature and then paraffin for 1 h at 55 °C. The tissue was then embedded, and 5-μm thick sections were prepared using a Microm (Baxter Scientific) microtome and placed on super-frost plus slides (Fisher). Slides were then hematoxylin and eosin-stained according to standard laboratory protocols.

Quantitation of Nuclei—Wild-type and Cav-1 null mouse lung tissue sections stained with hematoxylin and eosin were examined using a Zeis Axiophot. By using a 20× objective, six random 0.5-mm^2 fields were photographed for each genotype, and all the nuclei within those regions were manually tabulated using a hand-held counter.

Immunostaining of Lung Paraffin Sections—Sections of wild-type and Cav-1 null mouse lung were de-paraffinized in xylene for 4 min and rehydrated through a graded series of ethanol and placed in PBS. Sections were pre-blocked with 2% horse serum for 20 min and then washed with PBS for 10 min. The sections were incubated with a given primary antibody at room temperature for 1 h. An FITC-conjugated or lissamine-rhodamine-conjugated secondary antibody was added to the sections after a 10-min wash in PBS. After a 30-min incubation with the secondary antibody, the sections were washed in PBS for 20 min. Prolong anti-fade reagent was then added to prevent bleaching of the fluorochrome. Samples were imaged with an Olympus IX 70 inverted microscope. Anti-VEGF-R IgG (Flk-1; rabbit pAb C-20) was purchased from Santa Cruz Biotechnology, Inc. Anti-Ki67 IgG (rabbit pAb; NCL-Ki67p) was purchased from Novocastra, Ltd, UK, and used at a dilution of 1:500. For Ki67 immunostaining, sections were subjected to antigen retrieval by microwave irradiation in 0.01 M, pH 6, trisodium citrate buffer.

Assessment of Exercise Tolerance—A 4-liter beaker filled with water (25 °C) was used as a "swimming pool" to assess the exercise tolerance of male mice. Briefly, a very light weight (a paper clip; 0.4 g; ~1.25% of their body weight) was attached to the tail of a mouse with a body weight of ~32 g. The mouse was gently placed in the water and carefully observed. The time at which the mouse was initially unable to maintain complete buoyancy was recorded and the mouse was immediately removed from the pool. No mice were injured in these experiments; 5 animals were tested for each genotype.

Aortic Ring Studies of Vasoconstriction and Vasorelaxation—Wild-type and Cav-1 null male mice (4.5 months old) were sacrificed by CO_2 asphyxiation. The thoracic aorta was dissected and cut into cylindrical segments of ~3 mm in length. Five to six rings from 3 mice were obtained from each genotype of mouse strain. Rings were immediately placed in ice-cold Krebs-Henseleit buffer containing the following composition (in mM): NaCl, 110, KCl, 4.8, $CaCl_2$, 2.5, $MgSO_4$, 1.2, KH_2PO_4, 1.2, $NaHCO_3$, 25, glucose and dextrose, 11, in glass-distilled water. Briefly, the rings were suspended by two hooks (25-μm thickness) inserted into the lumen and mounted in a vessel myograph system (7-ml organ bath, Danish Myo Technology, Aarhus, Denmark) containing Krebs-Henseleit buffer. The organ chambers were maintained at 32 ± 0.05 °C and continuously bubbled with 95% O_2 and 5% CO_2 to maintain pH 7.4 ± 0.1. The mouse aortas were submitted to a resting tension of 1.2 g, and isometric tension was recorded using a transducer coupled to a MacLab data acquisition system. Following a 60-min equilibration period, with frequents washings (every ≈15 min), the rings were preconstricted with a submaximal concentration of PE (10 μM), and concentrations of Ach (10^{-8} to 10^{-4} M) or L-NAME (100 μM) were injected when the PE-contractile response achieved steady state (≈5 min).

Data are expressed as means ± S.E. Statistical differences were measured by one-way analysis of variance followed by Newman-Keul post-hoc test.

RESULTS

Generation of Caveolin-1-deficient Mice via Targeted Disruption of the Cav-1 Locus—We previously determined the genomic organization of the caveolin-1 (Cav-1) locus and found that exons 1 and 2 are spaced within 2 kb of each other, whereas exon 3 is ~10 kb downstream (47). Therefore, we generated a targeting vector designed to replace the first two exons and a small portion of the 5′ promoter sequence with the neomycin resistance cassette (*neo*) (Fig. 1*A*).

WW6 embryonic stem (ES) cells (56) were electroporated with the targeting vector, and 360 clones were selected with G418. Homologous recombination at this locus is predicted to create two new restriction sites, *Pst*I and *Xba*I, both of which can be used to identify positive ES cell clones by Southern blot analysis (Fig. 1*A*); four clones were determined to be positive in this manner. Germ line chimeras were derived from only two of these clones, as shown in the positive Southern blots in Fig. 1*B*. We subsequently mated these chimeras with C57Bl/6 mice to yield F1 heterozygous offspring, a cohort of which was interbred to produce the Cav-1 null progeny. Southern blot and PCR-based methods of assessing the targeted locus were performed on the first series of live offspring, confirming the predicted loss of a wild-type 8.0-kb band on Southern blot and the 500-bp band on PCR analysis (Fig. 1*C*). Genotyping of offspring from such heterozygous inter-crosses revealed that there is no reduced viability of the Cav-1-null mice and that mice of all three genotypes are present at the expected Mendelian frequency (Cav-1+/+ 25.2%, Cav-1 +/− 49.2%, Cav-1−/− 25.6%; n = 305 animals).

Although Cav-1 is expressed in numerous tissues at varying levels, it is found in abundance in certain terminally differentiated cells (*i.e.* adipocytes, endothelial cells, type I pneumocytes, and fibroblasts) (9, 11). Furthermore, Cav-1 expression is completely absent in skeletal and cardiac muscle cells, and in contrast, caveolin-3 (Cav-3), another member of the caveolin gene family, is selectively expressed (10, 12). In order to verify whether the targeted disruption of the Cav-1 locus led to a truly null mutation, we determined the expression of the Cav-1 protein in adipose, lung, and heart tissues from mice of all three genotypes (wild-type, heterozygote, and knockout; Fig. 1*C*). In all tissues examined, ablation of the Cav-1 locus leads to a concomitant loss of Cav-1 protein expression; β-tubulin is shown as an equal protein loading control.

In addition, several points are worth noting. 1) These mice are deficient in both Cav-1 isoforms (the full-length 178-amino acid α-isoform and the shorter 146-amino acid β-isoform (52)). 2) The ablation of the Cav-1 locus in only one chromosome, as in the heterozygous animals, is sufficient to reduce protein levels by approximately half. 3) Although Cav-1 is expressed in the cardiac tissue of wild-type and heterozygous mice (Fig. 1*D*), Cav-1 expression is derived from endothelial and fibroblastic cells within the heart and not the cardiac myocytes themselves (10, 12).

We also assessed Cav-1 expression in cultured mouse embryonic fibroblasts (MEFs), another cell type with abundant Cav-1 expression (67). Two different clones of MEFs for each possible genotype were extracted and cultured from day 13.5 embryos. Immunoblot analysis of Cav-1 levels indicated similar findings to those above, namely a complete ablation of Cav-1 expression in the knockout and a significant reduction in Cav-1 expression in heterozygous MEFs (Fig. 1*E*).

Phenotype and Histopathological Examination of Cav-1−/− Mice—Caveolin-1 null mice are both viable and fertile. We initially established a large cohort consisting of mice from all genotypes, the eldest of which are now 9 months of age. Although no overt phenotypic abnormalities (including tumors) have been detected, only two mice have thus far died of unknown causes, both of which were Cav-1-deficient (autolysis prevented a pathological work-up). Follow-up of this cohort in the coming months will establish whether Cav-1 deficiency can precipitate tumorigenesis and/or a reduction in life span. A routine histopathological examination of Cav-1 null mice at 4–5 months of age (n = 4 male, n = 4 female) failed to show any evidence of abnormalities, with the exception of lung tissue (see below). We have noticed, however, that although in the first few months of life there is no overt difference between wild-type and knockouts, older Cav-1-deficient mice are more likely to be smaller in size than their wild-type littermates.

The Absence of Caveolin-1 Is Sufficient to Abrogate Caveolae Formation—The molecular components required for caveolar biogenesis have been studied by numerous investigators. From the following observations, the general consensus remains that caveolin-1 plays an essential role in caveolae formation. 1) Cholesterol is required for caveolar invagination, because treatment with cholesterol-depleting agents (*e.g.* filipin and methyl-β-cyclodextrin) ablates caveolar structures (68). 2) Caveolin-1 is a cholesterol-binding protein, possibly facilitating the concentration of the critical mass of cholesterol required for invagination (8, 69). 3) Down-regulation of caveolin-1 in Ha-

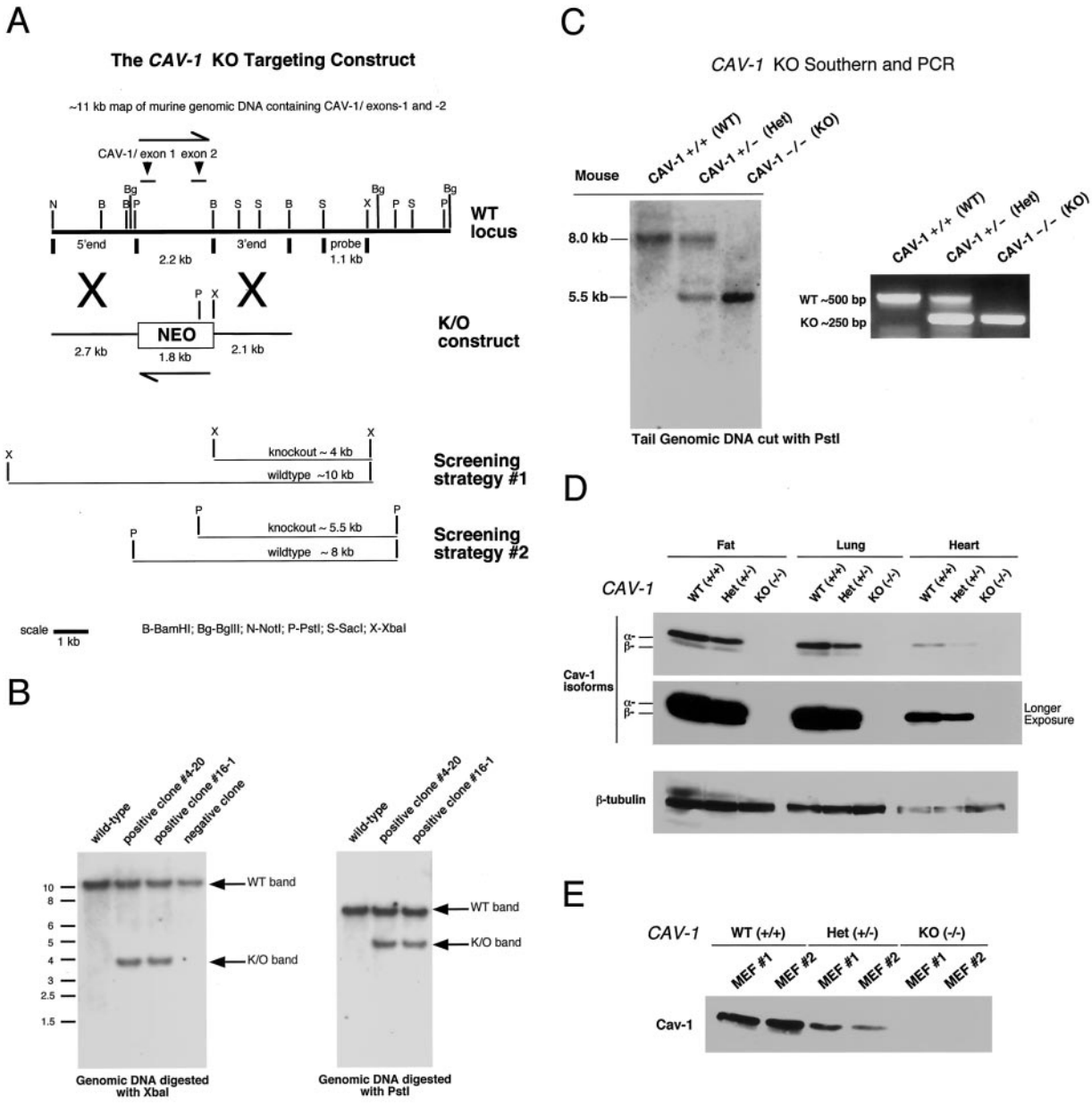

FIG. 1. **Targeted disruption of the *cav-1* gene produces a null mutation.** *A,* the Cav-1 locus (containing the first two exons) and the targeting construct (containing the neomycin (*NEO*) cassette with flanking segments homologous to the locus) are shown in schematic format. The transcriptional orientation of neomycin cassette and the Cav-1 locus are delineated by *arrows.* Note that homologous recombination would eliminate a 2.2-kb genomic segment containing Cav-1 exons 1 and 2 and introduce two new restriction sites (*Pst*I and *Xba*I), both of which can be used to screen for positive ES clones. The 1.1-kb *Sac*I-*Xba*I probe used for Southern blot analysis is located 3′ of the targeting vector, as shown. *B,* Southern blot analysis of two positive and wild-type ES cell clones. The probe used is a 1.1-kb *Sac*I-*Xba*I fragment located 3′ of the targeting vector shown in *A*. The 4-kb (*Xba*I digest) or 5.5-kb (*Pst*I digest) bands signify appropriate targeted disruption of the Cav-1 locus. *C,* Southern blot analysis of *Pst*I-digested tail DNA from the offspring of Cav-1 heterozygote inter-crosses. The absence of a wild-type 8.0 kb signifies the generation of the Cav-1 knockout animal. An alternative PCR-based strategy used to determine the genotype of animals is also shown. The absence of a 500-bp wild-type band signifies the generation of a Cav-1 knockout animal. *D,* lysates from three tissues with varying levels of Cav-1 expression (fat, lung, and heart) were prepared from mice of all three genotypes. 30 μg of protein was loaded in each lane, subjected to SDS-PAGE, and immunoblotted with anti-Cav-1 mAb (clone 2297). A longer exposure of the same blot fails to detect any Cav-1 expression in knockout tissues. Equal protein loading was assessed using the anti-β-tubulin mAb (clone 2.1). *E,* MEFs were derived from 13.5-day-old embryos. Two independent embryos of each genotype were selected for subsequent analysis. 20 μg of cell lysate was loaded in each lane, subjected to SDS-PAGE, and immunoblotted with anti-Cav-1 mAb (clone 2297).

Ras and v-Abl-transformed NIH 3T3 fibroblasts or by antisense strategies results in a concomitant reduction of caveolae at the membrane (28, 48). 4) Overexpression of caveolin-1 in a lymphocytic cell line, cells that do not endogenously express the protein, is sufficient to allow the formation of caveolae (6).

Thus, the generation of caveolin-1 null mice provided an opportunity to test this assertion under physiological conditions. In this manner, nonspecific effects due to chemical treatments, cellular transformation, and overexpression would not confound such a study. MEFs derived from Cav-1+/+ and −/− embryos were cultured to near 100% confluency, conditions that have been shown to result in optimal caveolin-1 expression and caveolae formation. Standard transmission electron microscopy was used to visualize the plasma membrane (Fig. 2). While wild-type MEFs have numerous uniformly sized caveolae, the Cav-1-deficient cells are conspicuously devoid of caveolae. An exhaustive search of the plasma membrane from Cav-1 knockout MEFs failed to show any invaginations resembling

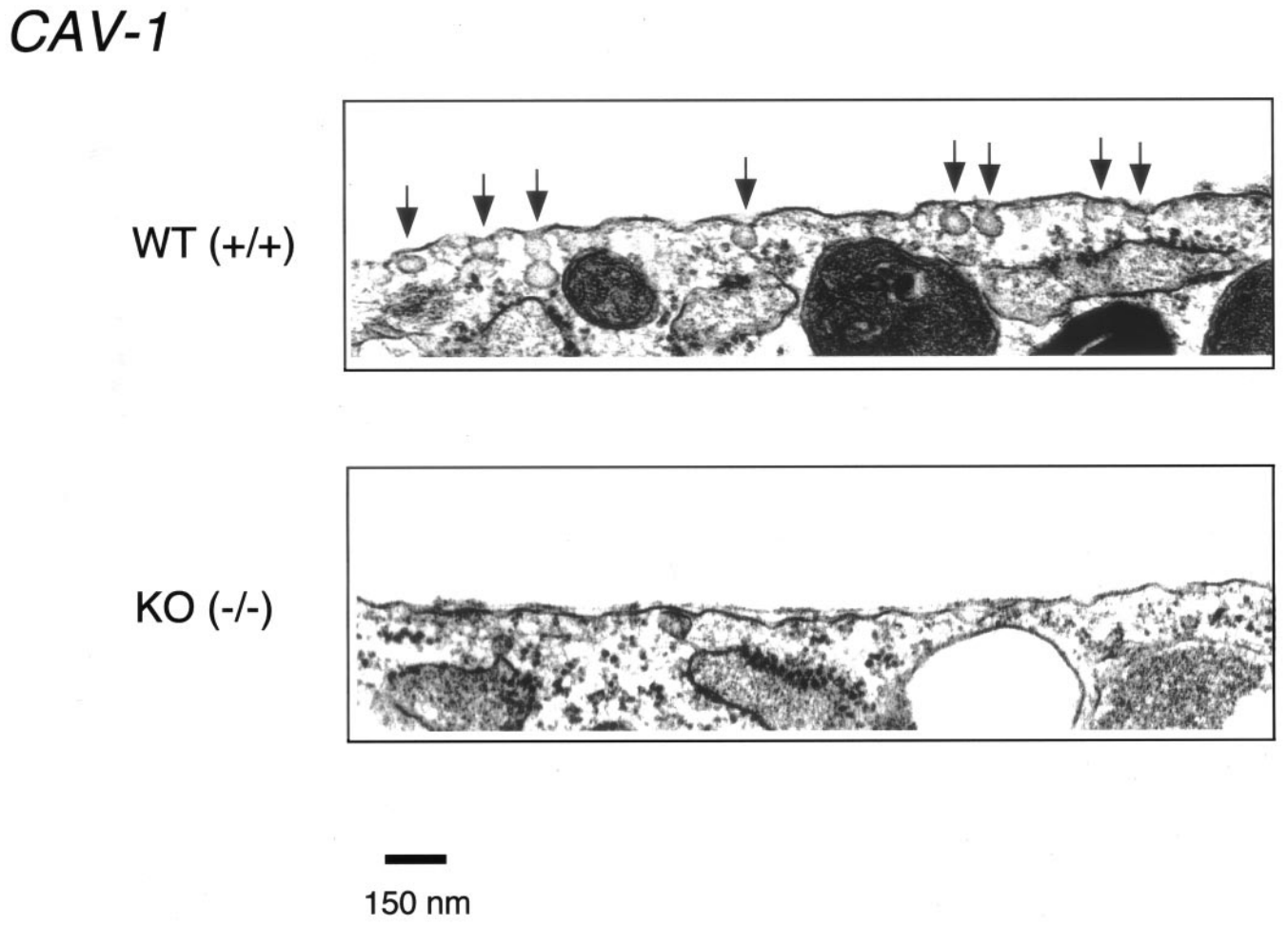

FIG. 2. **A deficiency in Cav-1 is sufficient to disrupt caveolae formation.** Cav-1 wild-type and knockout MEFs were grown to near-confluence on 60-mm dishes and prepared for transmission electron microscopy as described under "Experimental Procedures." All analyses were performed at × 16,000 magnification (for ease of view, images shown are further magnified to × 43,500). The plasma membranes of numerous cells were exhaustively scanned for caveolae, defined as uniform 50–100-nm flask-shaped membrane invaginations. The scale bar is shown at the *lower left corner* (*bar,* 150 nm).

caveolae. However, we did observe the occasional clathrin-coated pit (invaginations typically 5 times larger than caveolae) in MEFs of both genotypes (data not shown), indicating that their number or presence is not affected by a Cav-1 deficiency.

The Absence of Caveolin-1 Leads to Degradation and Redistribution of Caveolin-2—Currently, the caveolin gene family is composed of caveolin-1, -2, and -3. All known terminally differentiated tissues that express caveolin-1 also express the closely related family member caveolin-2 (Cav-2) (9, 11). In contrast, caveolin-3 (Cav-3), the protein with the highest homology to Cav-1, is expressed specifically in muscle cells (including cardiac, skeletal, and smooth muscle). Therefore, we were interested to determine any possible counter-regulatory or compensatory behavior by Cav-2 and Cav-3 in Cav-1 null tissues. We immunoblotted the same tissues samples used to compare Cav-1 expression in mice of different genotypes (Fig. 1*D*) for Cav-2 and Cav-3.

To our surprise, Cav-2 expression was greatly reduced in all the Cav-1(−/−) tissues examined (Fig. 3*A*). A longer exposure of the same blots shows that caveolin-2 is in fact expressed, albeit at ~5% of wild-type levels. Cav-3 levels remained unperturbed, however, and showed the expected expression pattern (*i.e.* muscle-specific expression) (Fig. 3*A*). A β-tubulin immunoblot indicates equal protein loading in all lanes (Fig. 3*A*). More importantly, in heterozygous animals, Cav-2 levels remain unperturbed despite the reduction in caveolin-1 (Fig. 1, *D* and *E*). Similar results were observed in Cav-1-null MEFs (Fig. 3*B*). Therefore, it seems that the absence, but not the reduction of Cav-1, is sufficient to cause a near-total deficiency in Cav-2.

The *in vivo* relationship between these two proteins (Cav-1 and Cav-2) goes beyond simple co-expression however. Although Cav-1 is able to form homo-oligomers consisting of 14–16 individual molecules (70, 71), it also is capable of forming similar size hetero-oligomers with Cav-2 (11, 72) and co-localizes with Cav-2 in caveolae microdomains (11). Additionally, it appears that Cav-2 requires the presence of Cav-1 for oligomerization and plasma membrane localization; when Cav-2 is overexpressed alone, it behaves as a mixture of monomers and dimers and is found in the Golgi complex (73–75). However, down-regulation of caveolin-1 either by antisense strategies or by oncogenic transformation (conditions where Cav-1 is reduced to undetectable levels) has no effect on Cav-2 levels or their localization (48).[2] The generation of Cav-1-deficient mice provided us the opportunity to definitively resolve the relationship between Cav-1 and Cav-2 *in vivo*.

Due to the abundance of Type I pneumocytes and endothelial cells, lung tissue is a great source for the purification and molecular analysis of caveolae (60). In order to determine the localization of Cav-2 in Cav-1 null mice, we subjected mouse

[2] B. Razani, J. A. Engelman, X. B. Wang, W. Schubert, X. L. Zhang, C. B. Marks, F. Macaluso, R. G. Russell, M. Li, R. G. Pestell, D. Di Vizio, H. Hou, Jr., B. Knietz, G. Lagaud, G. J. Christ, W. Edelmann, and M. P. Lisanti, unpublished observations.

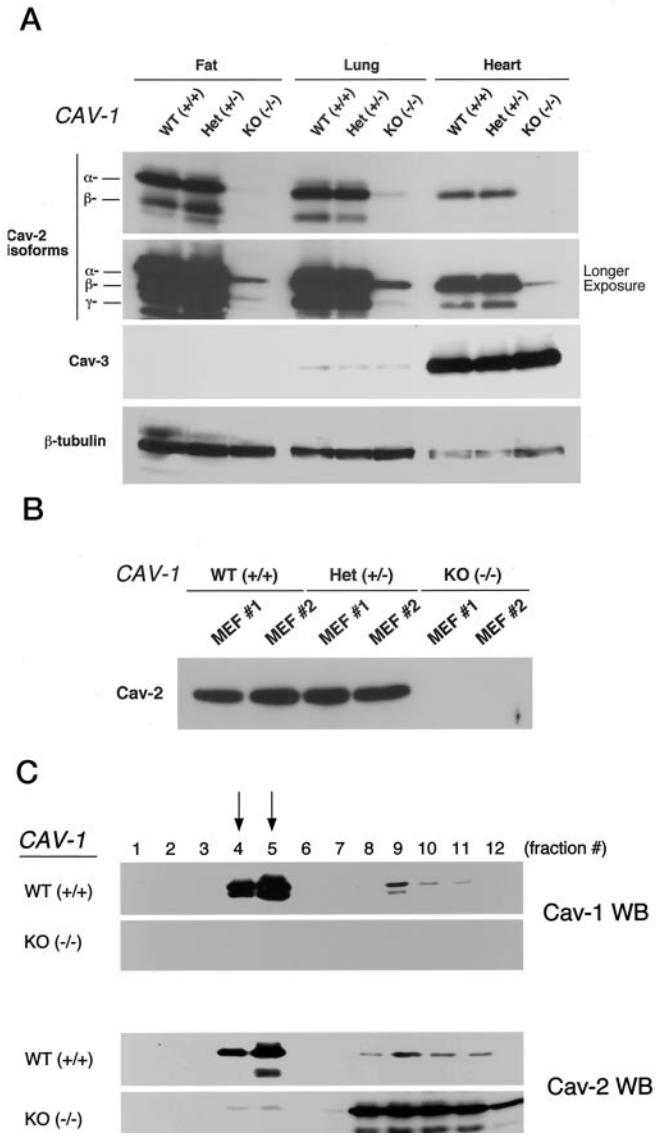

FIG. 3. **Phenotypic behavior of the caveolin-2 protein in Cav-1 null cells.** *A* and *B,* the absence of Cav-1 leads to severely reduced caveolin-2 levels. *A,* 30 μg of lysates from tissues used in Fig. 1*D* were loaded in each lane, subjected to SDS-PAGE, and immunoblotted with anti-Cav-2 mAb (clone 26) and anti-Cav-3 mAb (clone 65). A longer exposure of the same blot shows that Cav-2 is expressed in Cav-1 knockout mice, albeit at extremely reduced levels (~5% of wild-type). Equal protein loading was assessed using the anti-β-tubulin mAb (clone 2.1). Note that the expression of caveolin-3 remains muscle-specific. *B,* 20 μg of lysates from MEFs used in Fig. 1*E* were subjected to SDS-PAGE and immunoblotting with anti-Cav-2 mAb (clone 26). *C* and *D,* caveolin-2 is displaced from caveolae microdomains and localizes to a perinuclear compartment in Cav-1 null cells. *C,* lung tissue from wild-type and knockout mice was homogenized thoroughly in lysis buffer containing 1% Triton X-100 and subjected to sucrose gradient centrifugation, a procedure that separates caveolar microdomains from other cellular constituents (60). Twelve fractions, of which fractions 4–5 and 8–12 are considered of caveolar and non-caveolar origin, respectively, were collected and subjected to SDS-PAGE. Immunoblotting with anti-Cav-1 mAb (clone 2297) and anti-Cav-2 mAb (clone 26) was used to determine the localization of Cav-1 and Cav-2 in these gradient fractions. Note that the Western blot showing the distribution Cav-2 in Cav-1 null lung tissue is overexposed to illustrate the distribution of residual Cav-2, as Cav-2 protein levels are down-regulated to ~5% of normal levels in Cav-1 null animals. *D,* formaldehyde-fixed wild-type and knockout MEFs were doubly immunostained with anti-Cav-1 pAb (N20) and anti-Cav-2 mAb (clone 26). Bound 1° antibodies were visualized with distinctly tagged 2° antibodies (see "Experimental Procedures"). Note the perinuclear/Golgi localization of caveolin-2 in Cav-1 knockout MEFs.

lung tissue to extraction and sucrose gradient ultracentrifugation, a procedure with which we have previously separated caveolar microdomains from other cellular constituents. Via this method, it is possible to dramatically concentrate Cav-1, the caveolae marker protein, with respect to total cellular protein (60, 62). The outputs of this centrifugation consist of 12 equal fractions (of which fractions 4–5 and 8–12 are considered of caveolar and non-caveolar origin, respectively). As shown in Fig. 3*C*, Cav-1 and -2 are enriched heavily in the caveolar fractions of wild-type lungs. Interestingly, however, in Cav-1-deficient lungs, Cav-2 is almost entirely excluded from such fractions. We also obtained similar results in cultured MEFs (data not shown), indicating that a lack of Cav-1 alters the fractionation of Cav-2.

We next attempted to uncover more definitively the subcellular localization of Cav-2. Fig. 3*D* shows a series of micrographs of wild-type and knockout MEFs co-immunostained with anti-Cav-1 polyclonal and anti-Cav-2 monoclonal antibodies. There is a distinct and overlapping membrane localization for Cav-1 and -2 in wild-type cells; in contrast, we found Cav-2 only in the perinuclear Golgi compartments of Cav-1-deficient MEFs (Fig. 3*D*). We reasoned that transient transfection of these Cav-1 knockout cells with the Cav-1 cDNA should rescue and redistribute Cav-2 away from the Golgi, restoring its plasma

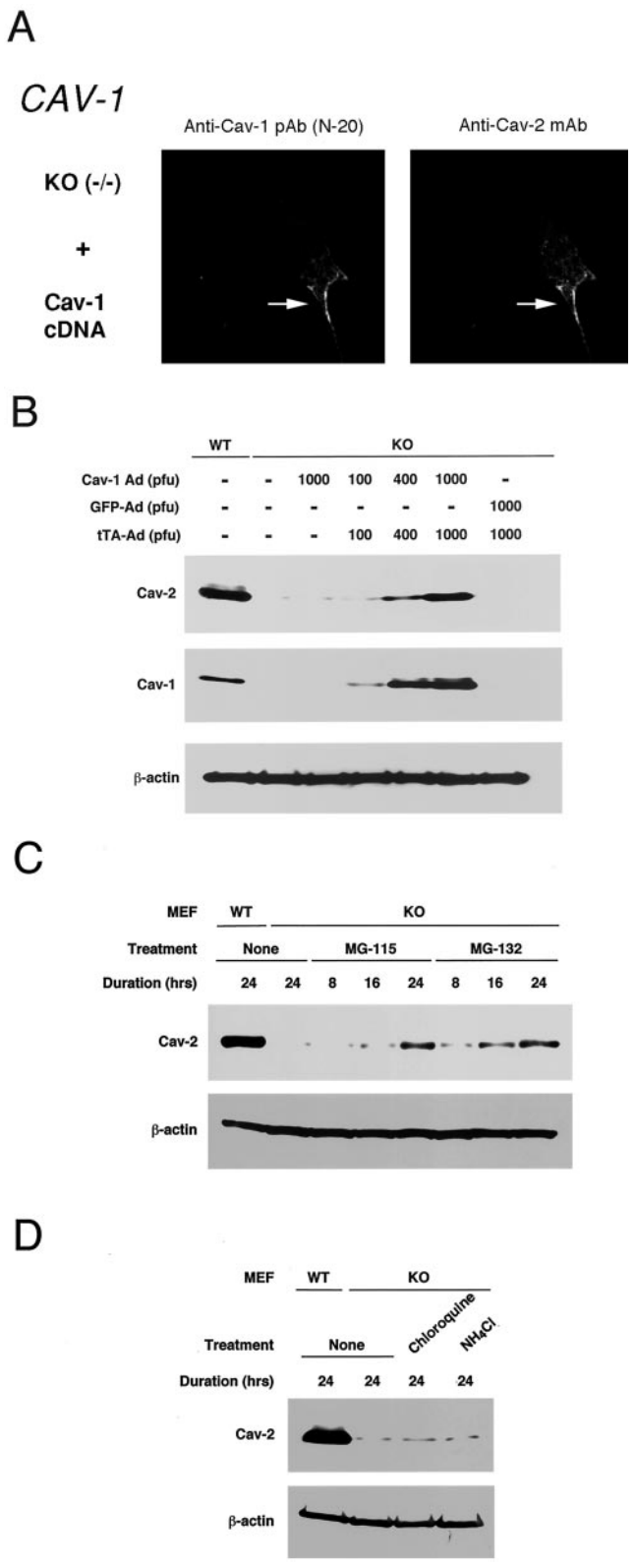

FIG. 4. **Rescue of caveolin-2 expression in Cav-1 null cells.** *A* and *B,* caveolin-2 localization and expression can be rescued by recombinantly expressing Cav-1 in Cav-1 knockout cells. *A,* Cav-1−/− MEFs were transiently transfected with the full-length cDNA encoding Cav-1. Thirty six hours post-transfection, cells were formaldehyde-fixed and doubly immunostained with anti-Cav-1 pAb (N20) and anti-Cav-2 mAb (clone 26) as in Fig. 3*D*. The image shown is that of a Cav-1-transfected cell. *B,* in order to obtain a higher efficiency of Cav-1 expression in Cav-1−/− MEFs, an adenoviral strategy was used (34). The Cav-1 and GFP adenoviruses (Ad-Cav-1 and Ad-GFP) contain a tet-responsive promoter that can only be induced by co-infection of cells with the tet-transactivator (Ad-tTA) – "tet off" system. MEFs were co-infected with Ad-Cav-1 and Ad-tTA at varying titers (100,400, and 1000 PFUs/cell). Controls included infection with Ad-Cav-1 alone (1000 PFUs/cell) or co-infection with Ad-GFP and Ad-tTA (1000 PFUs/cell). *C* and *D,* in the absence of Cav-1, caveolin-2 is partially degraded through the proteasomal pathway. *C,* Cav-1−/− MEFs grown to near-confluence were treated with the proteasomal inhibitors MG-132 (1 μM) and MG-115 (1 μM) for a series of time points (8, 16, and 24 h) or with vehicle (Me_2SO). Whole cell lysis and subsequent SDS-PAGE allowed the comparison of Cav-2 levels with that of wild-type MEFs. *D,* Cav-1(−/−) MEFs, grown to near-confluence, were treated with the lysosomal inhibitors chloroquine (50 μM) and NH_4Cl (10 mM) or vehicle (Me_2SO) for 24 h. Whole cell lysis and subsequent SDS-PAGE allowed comparison of Cav-2 levels with that of wild-type MEFs. Equal protein loading was assessed in *A* and *B* with anti-β-actin mAb (clone AC-15).

membrane localization. Fig. 4*A* confirms this assumption, showing co-localization of both proteins at the cell surface in the Cav-1 transfected cell. It should be noted that the Golgi staining for Cav-2 in neighboring untransfected cells is not viewable at this exposure simply due to the immensely reduced Cav-2 expression.

We have described previously a high efficiency method of Cav-1 overexpression using adenovirus-mediated gene transfer (34). With this strategy, we would be able to demonstrate biochemically a Cav-1-mediated rescue of Cav-2 expression. Since the Cav-1 adenovirus contains a tet-responsive promoter ("tet-off" system), Cav-1 expression is possible only by co-infection of cells with a tet-transactivator (tTA)-producing virus. Fig. 4*B* shows that a steadily increasing dose of adenoviral titers achieves a concomitant increase in Cav-1 expression. In turn, we observe a robust elevation of Cav-2 expression; β-actin is used as an equal protein loading control. Note that expression of equal titers of the irrelevant protein GFP have no effect on Cav-2 expression (Fig. 4*B*).

To gain insight into possible mechanisms for the reduction in Cav-2 levels, we focused on the cellular degradative machinery. The obvious requirement of Cav-1 for both the expression and membrane trafficking of Cav-2 indicates that protein misfolding, a hang-up in the Golgi, and subsequent degradation (proteasomal pathway) or an increase in retrograde trafficking from the membrane (lysosomal pathway) are possible areas of investigation. Therefore, we treated Cav-1 knockout MEFs with MG-132 and MG-115 (two classically used proteasomal inhibitors (76, 77)) and chloroquine and NH_4Cl (two lysosomal inhibitors) for a period of up to 24 h (Fig. 4, *C* and *D*). We discovered that only the proteasomal inhibitors have a positive effect on Cav-2 expression. Over a time course of 8, 16, and 24 h, Cav-2 levels increase substantially from base line. It is interesting to note, however, that the increase in Cav-2 expression is not complete. This could be due to the following: 1) sub-optimal dosages of proteasomal inhibitors, a condition not rectifiable in such experiments as higher dosages have toxic effects on the MEF cells[2] or 2) the presence of other degradative processes not fully abrogated by our repertoire of chemical inhibitors.

Caveolin-1 Null MEFs Show Defects in the Endocytosis of Albumin but Not Transferrin—Albumin has been used extensively to monitor caveolae-mediated endocytosis (78). Thus, we next examined the ability of Cav-1-deficient MEFs to endocytose the fluorescent tracer, FITC-albumin. Fig. 5, *A* and *B,* shows the Cav-1-deficient MEFs fail to accumulate FITC-albumin even after 30–60 min of continuous incubation. In contrast, wild-type MEFs show cell surface labeling with FITC-albumin after only 5 min, with significant intracellular accumulation by 15 min of incubation. These results support the idea that caveolae clearly participate in endocytosis of specific ligands, such as albumin. Importantly, transient expression of the caveolin-1 cDNA in Cav-1-deficient MEFs was sufficient to restore the uptake of FITC-albumin (Fig. 5*B*).

To ensure that a lack of caveolin-1 expression did not glo-

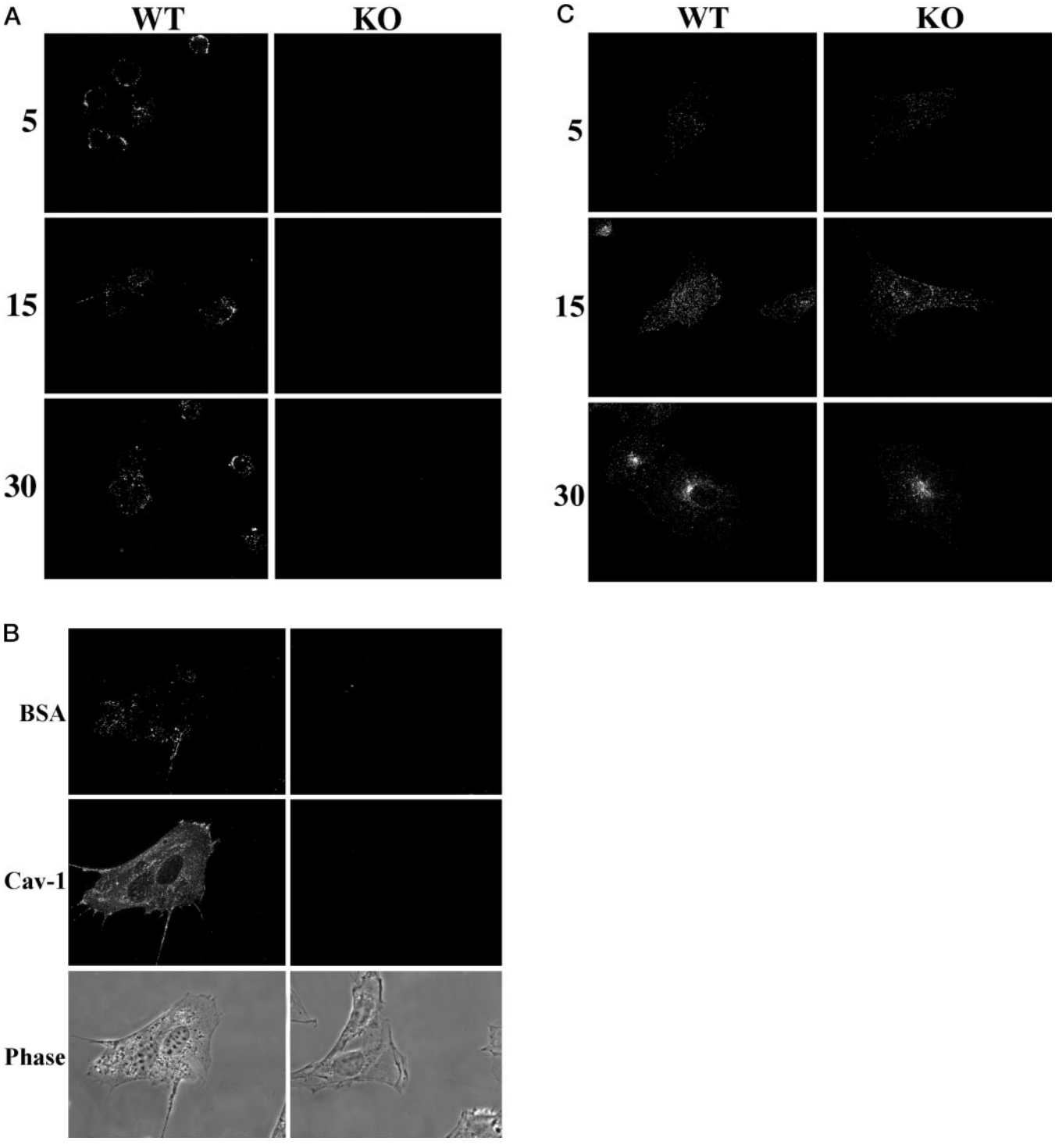

FIG. 5. **Caveolin-1-deficient MEFs show defects in the endocytosis of albumin but not transferrin.** *A,* wild-type and Cav-1 null MEFs were incubated in normal medium supplemented with FITC-albumin (10 μg/ml). After 5, 15, and 30 min at 37 °C, cells were formaldehyde-fixed and visualized by fluorescence microscopy. Note that Cav-1 null MEFs fail to internalize FITC-albumin. *Left panels*, wild-type MEFs (*WT*); *right panels*, Cav-1 null MEFs (*KO*). *B,* Cav-1 null MEFs were transiently transfected with the full-length cDNA encoding caveolin-1. Thirty six hours post-transfection, cells were allowed to continuously endocytose FITC-albumin for 30 min, as in *A*. Cells were then formaldehyde-fixed and immunostained with anti-Cav-1 IgG (rabbit pAb N-20). Note that in cells recombinantly expressing the caveolin-1 cDNA that uptake of FITC-albumin is clearly restored (*left panels*). However, untransfected cells in the same cell population failed to internalize FITC-albumin (*right panels*). *Upper panels,* FITC-albumin uptake; *middle panels*, Cav-1 immunostaining; *lower panels*, phase images. *C,* wild-type and Cav-1 null MEFs were incubated in normal medium supplemented with FITC-transferrin (10 μg/ml). After 5, 15, and 30 min at 37 °C, cell were formaldehyde-fixed and visualized by fluorescence microscopy. Note that both wild-type and Cav-1 null MEFs internalize FITC-transferrin, without any apparent differences. *Left panels,* wild-type MEFs (*WT*); *right panels,* Cav-1 null MEFs (*KO*).

bally affect endocytosis, we also examined the fate of a second fluorescent tracer, FITC-transferrin, which is endocytosed via clathrin-coated pits. Fig. 5*C* demonstrates that FITC-transferrin was rapidly endocytosed in both wild-type and Cav-1-deficient MEFs, with no apparent differences. After 30 min, FITC-transferrin accumulated in a perinuclear compartment in both wild-type and Cav-1-deficient MEFs.

Thus, Cav-1-deficient MEFs show a selective defect in the

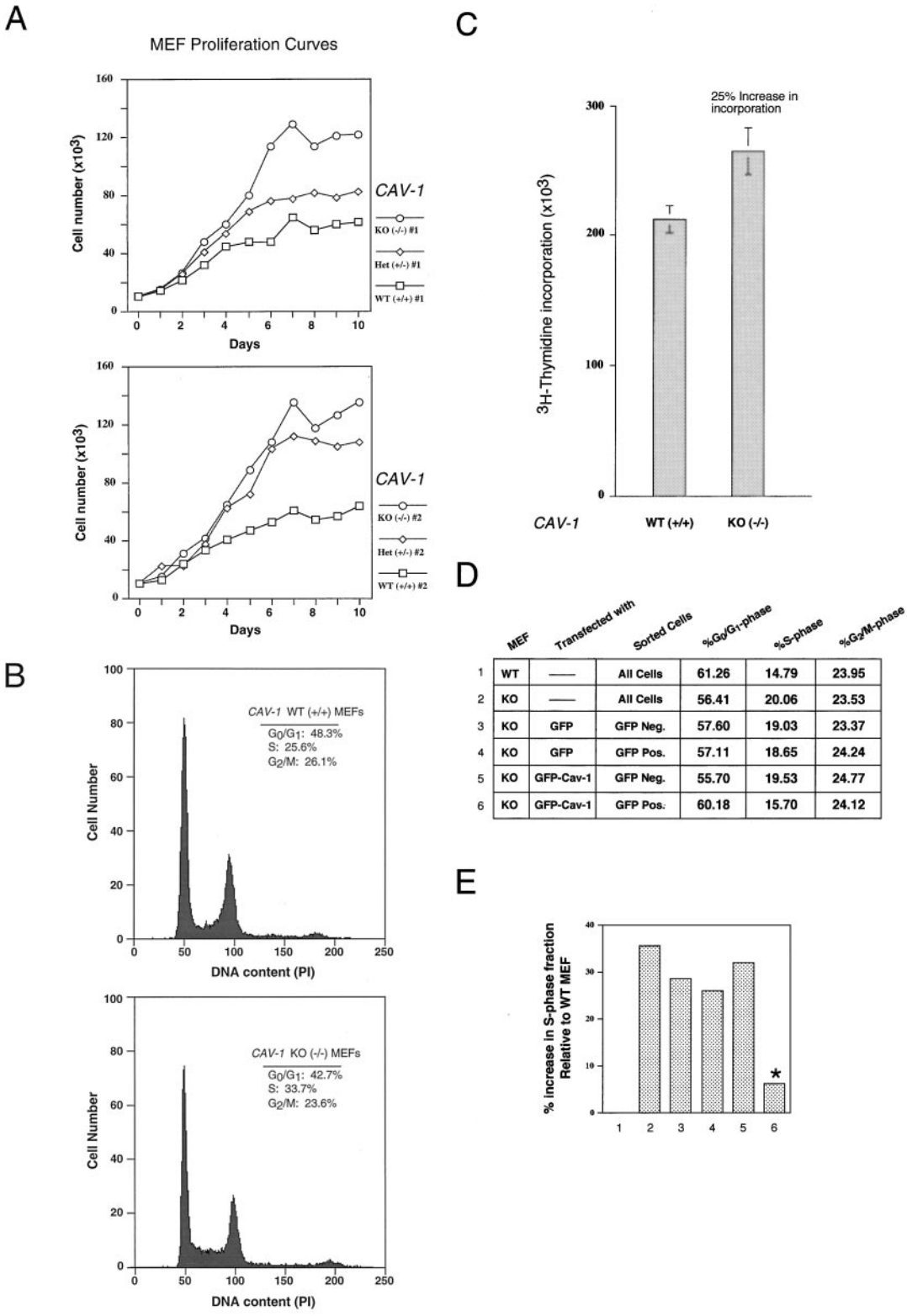

	MEF	Transfected with	Sorted Cells	%G0/G1-phase	%S-phase	%G2/M-phase
1	WT	—	All Cells	61.26	14.79	23.95
2	KO	—	All Cells	56.41	20.06	23.53
3	KO	GFP	GFP Neg.	57.60	19.03	23.37
4	KO	GFP	GFP Pos.	57.11	18.65	24.24
5	KO	GFP-Cav-1	GFP Neg.	55.70	19.53	24.77
6	KO	GFP-Cav-1	GFP Pos.	60.18	15.70	24.12

FIG. 6. **Growth properties and cell cycle analysis of Cav-1−/− MEFs.** *A–C,* Cav-1-deficient MEFs proliferate faster and have increased S phase fractions. *A,* six independent MEF cultures, consisting of two Cav-1+/+, two Cav-1+/−, and two Cav-1−/− genotypes, were plated at a density of 15×10^3 cells/dish on a series of 35-mm dishes. Duplicate plates from each MEF culture were then counted each day for a period of 10 days. Cell numbers at the indicated time points (*Days 1–10*) are the average of duplicate plates. *B,* wild-type and knockout MEFs were plated at a density of 2×10^5 in 60-mm dishes. At the exponential phase of growth they were ethanol-fixed, stained with propidium iodide, and analyzed by flow cytometry for the G_0/G_1, S, and G_2/M phases of the cell cycle. Parameters indicated are the percentage of cells in each phase of the cell cycle out of a total of 10,000 cells analyzed. *C,* wild-type and knockout MEFs were plated at a density of 2×10^5 in 60-mm dishes. Upon adherence to the plates they were supplemented with 1 μCi/ml [^{3}H]thymidine and cultured overnight. Incorporated tritium was determined by scintillation counts of alkaline lysed cells/trichloroacetic acid-precipitated DNA (see "Experimental Procedures"). Data shown are the average and standard deviation of counts from five plates. *D* and *E,* the increased S phase in Cav-1 null cells can be rescued by re-introduction of Cav-1. *D,* Cav-1 knockout MEFs were transfected with either GFP alone or GFP-Cav-1. Untransfected plates of wild-type and knockout cells were similarly cultured. Thirty six hours post-transfection, all cells were trypsinized, live-stained with Hoechst 33342, and subjected to flow cytometry. Transfected (*i.e.* GFP-positive) cells were distinguished from non-transfected cells (GFP-negative) by using appropriate fluorescence channels. Cell cycle

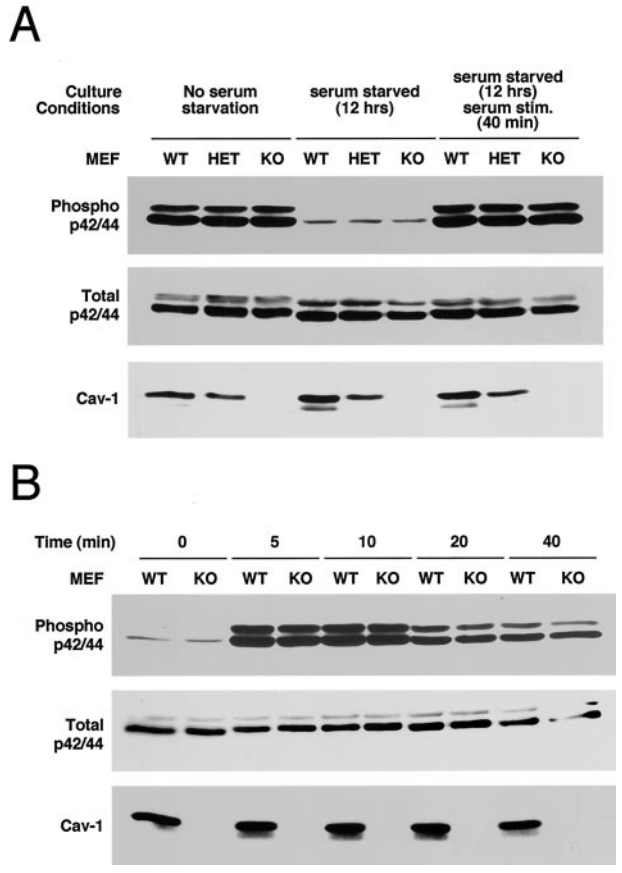

FIG. 7. **Hyperproliferation of Cav-1-deficient MEFs is not related to hyperactivation of the p42/44 MAP kinase cascade.** *A,* MEFs derived from embryos of all three genotypes were cultured in triplicate at 70–80% confluence. One set of cultures was grown continuously under normal serum conditions (DMEM, 10% FBS), and the other two were serum-starved for 12 h. Serum (10% FBS) was reintroduced into only one set of the serum-starved cells for 40 min. Cells were lysed, subjected to SDS-PAGE, and immunoblotted with phospho-specific anti-p42/44 pAb, anti-p42/44 antibody, and anti-Cav-1 mAb (2297). *B,* wild-type and knockout MEFs were plated in a series of 60-mm dishes, serum-starved for 12 h, and stimulated with EGF (50 ng/ml) for either 0, 5, 10, 20, or 40 min. Cells were lysed, subjected to SDS-PAGE, and immunoblotted for the same antibodies used in *A*.

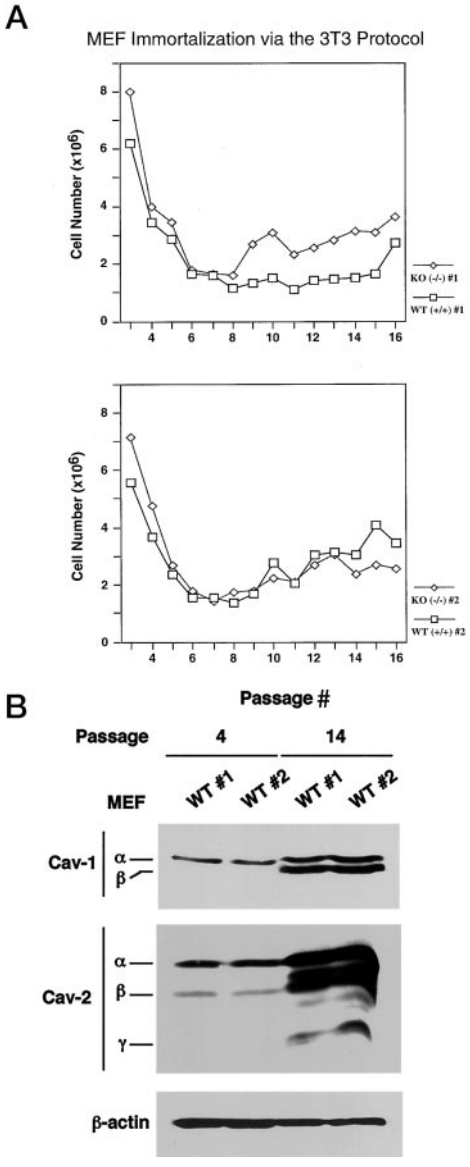

FIG. 8. **Although Cav-1 levels increase at higher passages of culture, the absence of Cav-1 does not impart an advantage in senescence and subsequent immortalization.** *A,* four independent MEF cultures (two wild-type and two knockout) were propagated according to the 3T3 protocol (*i.e.* 3×10^5 cells were plated in 60-mm dishes every 3 days). At each passage (2–16), the combined cell counts from three 60-mm dishes were determined for each MEF culture by hemocytometer. *B,* wild-type and Cav-1 knockout MEFs were propagated according to the 3T3 protocol (*i.e.* 3×10^5 cells were plated in 60-mm dishes every 3 days). Cell lysates were prepared from Passage 4 and Passage 14 MEFs, subjected to SDS-PAGE, and immunoblotted with anti-Cav-1 mAb (clone 2297), anti-Cav-2 mAb (clone 65), or anti-β-actin mAb (clone AC-15).

uptake of a known caveolar ligand, *i.e.* albumin. This is consistent with our observation that Cav-1-deficient MEFs lack morphological caveolae, as seen by transmission electron microscopy (Fig. 2).

The Growth Properties and Cell Cycle Analysis of Cav-1−/− MEFs—In the past decade, several important observations have implicated Cav-1 as a negative regulator of signaling pathways involved in pro-proliferative responses; as a result, Cav-1 has been suggested to function as a putative tumor suppressor. Caveolin-1 levels are drastically reduced upon oncogenic transformation of several cell lines (28–30, 33–37, 61). More importantly, overexpression of Cav-1 is sufficient to abrogate anchorage-independent growth in these transformed cells (29–32, 34, 61). Cav-1 also interacts with and negatively regulates several pro-proliferative signaling molecules, such as certain receptor-tyrosine kinases (including EGF-R, platelet-derived growth factor receptor, and Neu), Ha-Ras, c-Src, and phosphatidylinositol 3-kinase, among others (17, 18, 24–27). Finally, down-regulation of Cav-1 by an antisense strategy in NIH-3T3 fibroblasts leads to a tumorigenic phenotype, enabling the these cells to grow in soft agar and nude mice (48).

However, all of this work has been conducted in immortalized cell lines (*i.e.* cells that have perturbations in one or more genes important for controlling cell cycle progression), a situation that may confound the physiological behavior of Cav-1. Therefore, we attempted to study Cav-1 function in cellular proliferation in cultured primary MEFs. We first determined the growth potential of six independent MEF cultures (two

parameters for all populations were analyzed as shown. The indicated numbers represent the percentages of cells in each phase out of a total of 10,000 cells. *E,* the percentage of increase in S phase fraction as compared with wild-type MEFs for all transfected and untransfected cell populations analyzed in *D*.

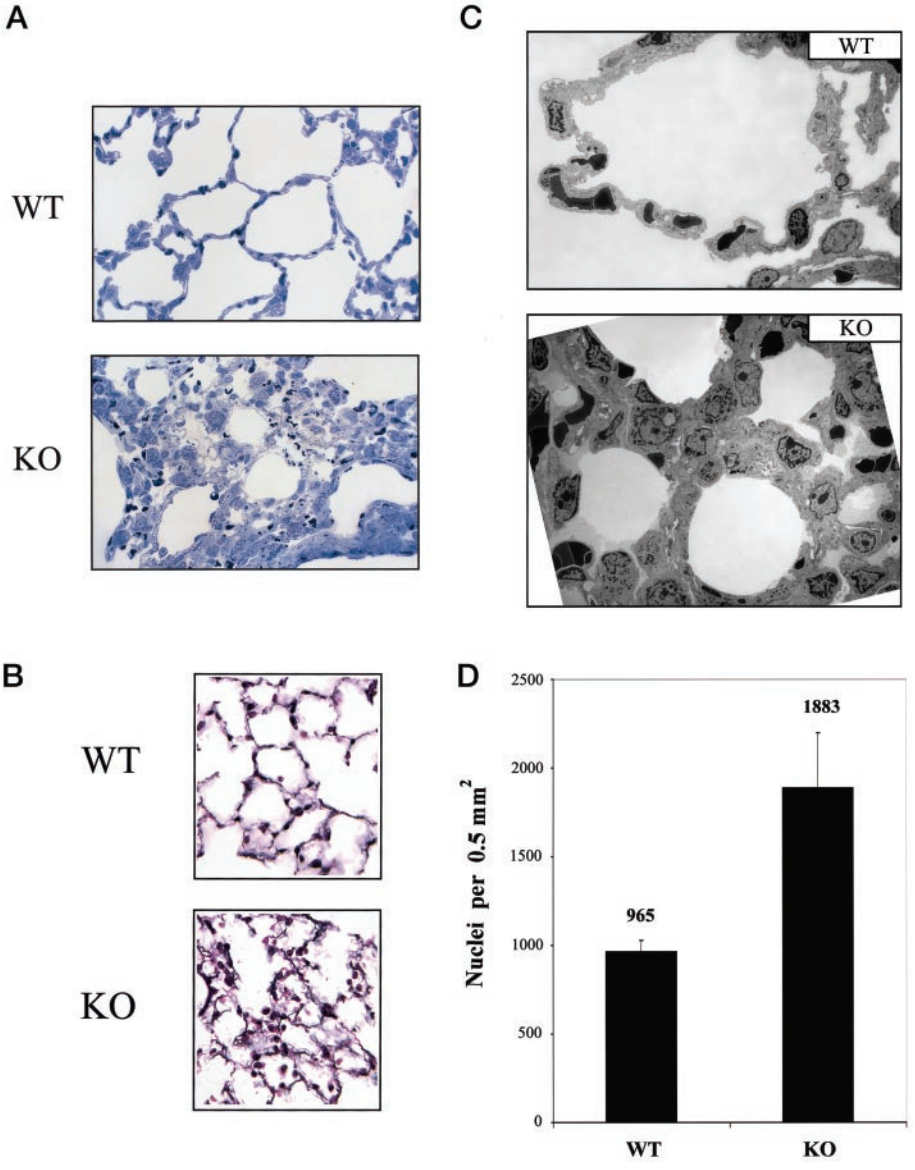

FIG. 9. **Caveolin-1-deficient mice show lung abnormalities, with thickened alveolar septa and hypercellularity.** *A,* light microscopy. One-μm sections of lung parenchyma were cut and stained with toluidine blue. Note that in caveolin-1-deficient mice the alveolar spaces appeared significantly smaller or appeared constricted, with thickened alveolar septa and hypercellularity. These images were acquired with a 60× objective. *Upper panel,* wild-type mice (*WT*); *lower panel,* Cav-1 null mice (*KO*). *B,* reticulin staining. Wild-type and Cav-1 null mouse lung tissue sections were subjected to reticulin staining and examined using a Zeis Axiophot with a 20× objective. Note that in caveolin-1-deficient mice, reticulin staining showed increased basement membranes in the thickened alveolar walls. There was increased density and thickness of the basement membranes and loose arrays of reticulin fibers. *Upper panel,* wild-type mice (*WT*); *lower panel,* Cav-1 null mice (*KO*). *C,* transmission electron microscopy. Lung tissue samples were processed for electron microscopy, as detailed under "Experimental Procedures." Images were acquired at low magnification (× 2,000), and montages were assembled to illustrate the detailed morphology of the alveolar architecture. Note the presence of thickened alveolar septa and hypercellularity in Cav-1-deficient mice. *Upper panel,* wild-type mice (*WT*); *lower panel,* Cav-1 null mice (*KO*). *D,* quantitation of nuclei. Wild-type and Cav-1 null mouse lung tissue sections stained with hematoxylin and eosin were examined using a Zeis Axiophot. Using a 20× objective, six random 0.5-mm^2 fields were photographed for each genotype, and all the nuclei within those regions were manually tabulated using a hand-held counter. Note that lung sections from Cav-1 null mice show an ~2-fold increase in overall cellularity.

from each possible genotype) (also shown in Figs. 1*E* and 3*B*) over a 10-day period. Cells were plated sparsely in a series of 35-mm dishes, two of which were counted each day. In each case, the Cav-1-deficient cells proliferated approximately 2-fold faster and to higher saturation densities than their wild-type counterparts (Fig. 6*A*). Remarkably, cells heterozygous for Cav-1 show intermediate proliferation rates that seem to inversely correlate with their levels of Cav-1 expression (see Fig. 1*E* for a comparison of Cav-1 protein levels). These experiments were also performed with MEFs derived from 2 other knockout and wild-type embryos with similar results (data not shown).

We next conducted a more quantitative growth comparison of the Cav-1+/+ and −/− cells. Fig. 6*B* shows a representative flow cytometric analysis of the cell cycle of wild-type and knockout MEFs in their exponential phase of growth. Note that there is a reproducible increase of ~25–30% in the S phase population of the Cav-1-deficient cells, with concomitant decreases in G_0/G_1 and to a lesser extent G_2/M. We quantitatively assessed this S phase increase in another way, *i.e.* by calculating the incorporation of [^{3}H]thymidine in randomly cycling wild-type and knockout MEFs. Fig. 6*C* shows the rates of S phase increase in line with the cell cycle analysis above (with increases in thymidine incorporation of ~25%). Interestingly, an increase in S phase of similar magnitude is observed in MEFs harboring a deletion of several classically known cell cycle inhibitors, such as p16^{INK4A}/p19^{ARF} and Rb (79, 80).

If increases in cellular proliferation and S phase are due to a Cav-1 deficiency, we reasoned that recombinant overexpression of Cav-1 in knockout cells should act to revert their cell cycle profiles to wild-type levels. In light of the fact that MEFs are relatively resistant to high transfection efficiencies, the following strategy was devised. We have described previously (63) the characterization of a GFP-Cav-1 chimera that behaves indistinguishably from wild-type Cav-1. Transient transfection of this GFP-Cav-1 chimera or GFP alone, followed by flow cytometric analysis of GFP-positive cells, allowed us to compare the cell cycle responses of transfected and untransfected cells. Fig. 6*D* summarizes the results from such an experiment, whereas Fig. 6*E* shows the relative changes in S phase between each group of cells. Note that expression of GFP alone was insufficient to complement the cell cycle defect in Cav-1−/− MEFs, whereas expression of GFP-Cav-1 successfully complemented this defect. Thus, we conclude that the observed increase in cell proliferation in Cav-1 null MEFs reflects a decrease in the number of cells in the G_0/G_1 phase of the cell cycle, with a corresponding proportional increase in the number of cells in the S phase.

The relative inability of Cav-1-deficient cells to control cel-

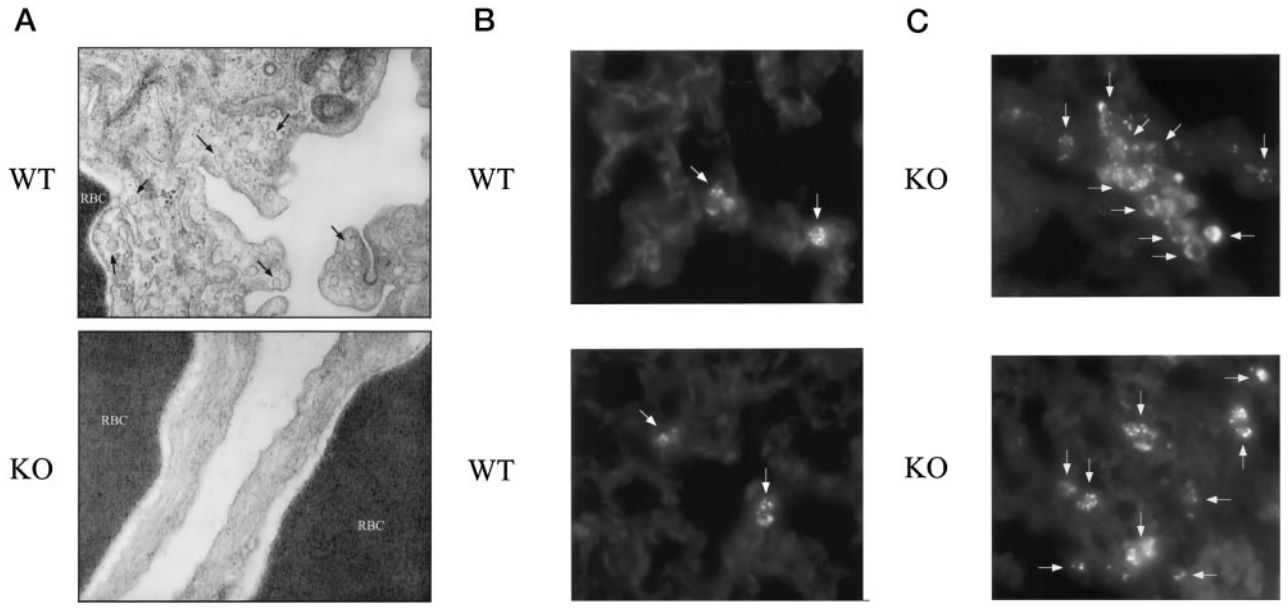

FIG. 10. **Lung endothelial cells in Cav-1-deficient mice lack caveolae and are more numerous.** *A,* transmission electron microscopy. Lung tissue samples were processed for electron microscopy as detailed under "Experimental Procedures." Images were acquired at high magnification (× 33,000). Note that endothelial cells from Cav-1 null mice lack caveolae, whereas their normal counterparts in wild-type mice showed abundant caveolae (see *arrows*). Endothelial cells were identified by their proximity to red blood cells (*RBC*) that are electron dense (due to their high iron content) and appear *black.* Similarly, type I pneumocytes also lacked caveolae in the Cav-1 null mice (not shown). *Upper panel,* wild-type mice (*WT*); *lower panel*, Cav-1 null mice (*KO*). *B* and *C,* immunostaining. Lung paraffin sections from wild-type and caveolin-1-deficient mice were immunostained with an endothelial marker, anti-VEGF-R (Flk-1) IgG. Bound primary antibodies were detected with a fluorescently labeled secondary antibody. *Arrows* point at VEGF-R-positive endothelial cells, which appear more numerous in lung sections from Cav-1-deficient animals. Two representative fields are shown for each genotype. *B*, wild-type mice (*WT*); *C,* Cav-1 null mice (*KO*). Long overexposures are shown to illustrate better the overall architecture of the adjacent VEGF-R-negative lung parenchyma.

lular proliferation could be a result of lost functional interactions with any of the signaling molecules previously implicated to interact with caveolin-1. Based on several important observations, one of the most attractive candidates in this process is the Ras/p42/44 MAP kinase signaling cascade. Cholesterol depletion of cellular membranes, a process that abolishes caveolae formation and Cav-1 membrane localization (3), leads to a hyperactivation of the p42/44 MAP kinase cascade (81). Antisense-mediated reductions of Cav-1 in NIH 3T3 fibroblasts leads to a similar hyperactivation of p42/44 MAP kinase cascade (48). Finally, the ablation of Cav-1 levels in *C. elegans* by RNA interference produces a meiotic phenotype that mirrors that of Ras activation (49). We attempted to recapitulate the above results in MEFs derived from wild-type and knockout embryos. Fig. 7*A* shows that under conditions of normal serum, serum starvation, and serum re-introduction (situations that activate, depress, and reactivate the p42/44 kinase cascade, respectively), Cav-1 deficiency does not affect the activation state of this cascade. We independently corroborated these results by observing a lack of altered kinetics in Cav-1-deficient cells under conditions of EGF-stimulated p42/44 phosphorylation (Fig. 7*B*). Therefore, we conclude that the hyperproliferative effect of Cav-1 deficiency on primary cultured cells is independent of the Ras/p42/44 MAP kinase cascade.

Caveolin-1 levels have previously been shown to increase at the onset of senescence in primary human fibroblasts (82). Therefore, we were interested in assessing the levels of Cav-1 in wild-type MEFs and the relative proliferation capacity of Cav-1 null MEFs at higher passages of culture. In this way, we could observe both the senescence and subsequent immortalization responses of Cav-1 knockout MEFs. By using a standard 3T3 passaging protocol, two wild-type and two Cav-1 knockout MEF cultures were serially propagated until immortalization. Fig. 8*A* shows the growth of these cells at each passage. There was no observable differences in senescence and subsequent immortalization in the Cav-1 null cells. We additionally performed immunoblot analysis on lysates taken from wild-type cells at passages 4 and 14 of culture. Fig. 8*B* shows a dramatic increase in Cav-1 and -2 expression at the higher passage, even though this phenomenon apparently does not appear to be important for age-dependent cellular senescence and growth arrest.

Caveolin-1-deficient Mice Show Lung Abnormalities, with Thickened Alveolar Septa and Hypercellularity, and Exercise Intolerance—As a consequence of the hyperproliferative phenotype we observed with Cav-1 null MEFs, we extensively examined our pathology specimens for evidence of hypercellularity. Interestingly, the lung appeared abnormal, and thin sections (1 μm) were cut to better evaluate this possible phenotype.

Fig. 9*A* shows toluidine blue-stained thin sections of lung parenchyma from wild-type and caveolin-1-deficient animals. Note that in caveolin-1-deficient mice, the alveolar spaces appeared significantly smaller or appeared constricted, with thickened alveolar septa and hypercellularity. In caveolin-1-deficient mice, reticulin staining showed increased basement membranes in the thickened alveolar walls (Fig. 9*B*). There was increased density and thickness of the basement membranes and loose arrays of reticulin fibers. However, lung fibrosis was not detected with trichrome staining (not shown). The presence of thickened alveolar septa and hypercellularity was indeed confirmed by transmission electron microscopy at low magnification. Montages of images taken of wild-type and Cav-1 null alveoli are shown in Fig. 9*C*.

As these lung tissue sections appeared hypercellular, we next quantitated the number of nuclei per high power field using hematoxylin and eosin-stained paraffin sections. Our results indicate that Cav-1 null mice lung sections show an ~2-fold increase in cellularity. This is consistent with our observation that Cav-1-deficient MEFs proliferate ~2-fold faster and to higher saturation densities than their wild-type counterparts (Fig. 9*D*).

As endothelial cells are one of the major cell types in lung tissue, and they are known to normally express high levels of

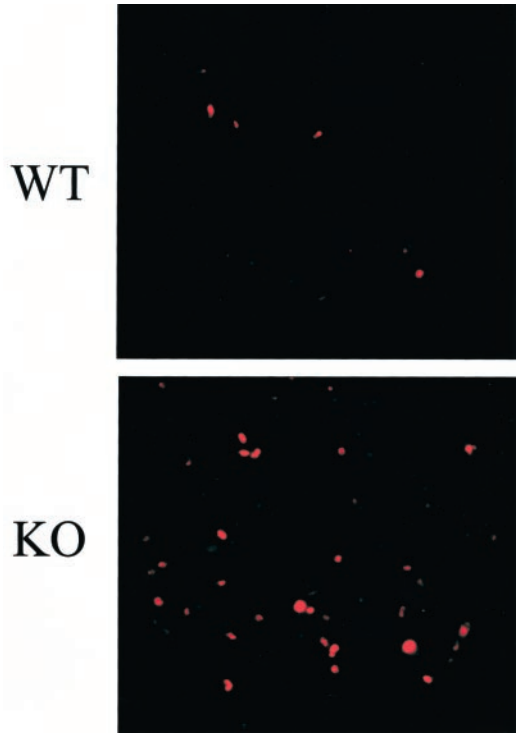

FIG. 11. **Immunostaining of the lung parenchyma with the Ki67 "proliferation" antigen.** Lung paraffin sections from wild-type and caveolin-1-deficient mice were immunostained with a widely used proliferation marker, Ki67. Bound primary antibodies were detected with a fluorescently labeled secondary antibody. Note that Ki67 immunoreactivity is dramatically increased in lung tissue sections from Cav-1 null mice, as compared with wild-type controls. *Upper panel,* wild-type mice (*WT*); *lower panel*, Cav-1 null mice (*KO*).

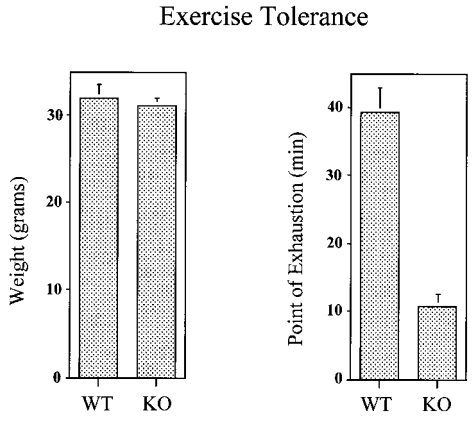

FIG. 12. **Exercise tolerance in wild-type and Cav-1-deficient mice.** Weight-matched, age-matched (4.5 months), same-sex littermates for each genotype were subjected to a "swimming test" (see "Experimental Procedures"). Note that wild-type animals were able to swim for up to 40 min, whereas Cav-1-deficient animals only swam for ~10 min (an ~4-fold change). Thus, Cav-1-deficient mice clearly show exercise intolerance, as would be predicted based on the morphology of the lung. Similar exercise intolerance was also observed in 1-month-old mice (not shown).

caveolin-1, we examined the status of lung endothelial cells in both wild-type and caveolin-1-deficient animals. Transmission electron microscopy revealed that endothelial cells from Cav-1 null mice lack caveolae, whereas their normal counterparts in wild-type mice showed abundant caveolae (Fig. 10*A*). We also used antibodies to VEGF-R (Flk-1) as a marker for endothelial cells. Immunostaining of paraffin sections with anti-VEGF-R revealed that the number of lung endothelial cells were increased in Cav-1 null animals. For example, in wild-type animals, we routinely observed ~1–2 VEGF-R-positive endothelial cells per 60× field, whereas in Cav-1-deficient animals there were ~6–10 VEGF-R-positive endothelial cells per 60× field. Also, in Cav-1-deficient animals, the VEGF-R-positive endothelial cells were sometimes present in discrete clusters, *i.e.* reminiscent of a focus of cellular growth. Two representative images for each genotype are shown in Fig. 10, *panels B* and *C*.

The Ki67 "proliferation" antigen is a nuclear protein that is highly expressed in proliferating cells (late G_1, S, G_2, and M phases of the cell cycle) and is undetectable in cells in the G_0 phase of the cell cycle (83, 84). Fig. 11 shows that Ki67 immunoreactivity is dramatically increased in lung tissue sections from Cav-1 null mice, as compared with wild-type controls. This is consistent with the idea that a lack of caveolin-1 can lead to hyperproliferation, as we have shown with Cav-1 null MEFs in culture (Fig. 6*A*).

To grossly assess the possible physical consequences of these lung abnormalities, we examined the exercise tolerance of wild-type and Cav-1-deficient mice. For this purpose, we subjected these animals to a "swimming test" (see "Experimental Procedures"). Fig. 12 shows that wild-type animals were able to swim for up to 40 min, whereas Cav-1-deficient animals only swam for ~10 min. Thus, Cav-1-deficient mice clearly show exercise intolerance when compared with their wild-type littermates.

Caveolin-1-deficient Mice Show Abnormal Vasoconstriction and Vasorelaxation Responses—Caveolin-1 is highly expressed in endothelial cells where caveolae are abundant. In addition, *in vitro* studies have shown that caveolin-1 functions as a tonic inhibitor of eNOS (85–87). Thus, we next assessed the vascular tone of isolated mouse aortic rings by using an established physiological method that measures tension in response to vasoconstriction or vasorelaxation.

For this purpose, we employed phenylephrine (PE; an α_1-adrenergic receptor agonist) as a vasoconstrictor and acetylcholine (Ach) to induce NO-dependent relaxation. To demonstrate a role for eNOS in these physiological responses, we took advantage of the availability of a well characterized arginine-based NOS inhibitor, known as L-NAME (nitro-L-arginine methyl ester).

As shown in Fig. 13, aortic rings isolated from the Cav-1 null mice were significantly different from their wild-type counterparts in all parameters examined. The results of a representative experiment on an aortic ring from each genotype (WT *versus* KO) are shown in Fig. 13*A*. As illustrated, PE was first used to elicit a contractile response. Upon achieving steady-state, relaxation was induced by adding acetylcholine (Ach) in gradually increasing doses (from 10^{-8} to 10^{-4} M), thereby creating a dose-response curve. Finally, in order to dissociate the PE-induced contractility from NO-mediated relaxation, the NOS inhibitor L-NAME was added to all rings.

There are several important observations to note. 1) The steady-state maximal tension response to PE in the wild-type aortic rings was nearly 2-fold greater than that observed for the Cav-1 null aortic rings (Fig. 13*B*, $p < 0.05$). It should be noted that over the same experimental time course, there was a less than 10% variation in tension development in wild-type and Cav-1 null aortic rings. 2) Although Ach induced a concentration-dependent relaxation response in aortic rings from both wild-type and Cav-1 null mice, significantly greater relaxation was observed in Cav-1 null aortic rings at all Ach concentrations examined (Fig. 13*C*). 3) After addition of L-NAME, the steady-state contractile response in the continuing presence of PE was significantly greater in aortic rings from both the wild-type and Cav-1 null mice; however, the percent increase was significantly greater for the Cav-1 null mice (see Fig. 13, *A* and *B*). Moreover,

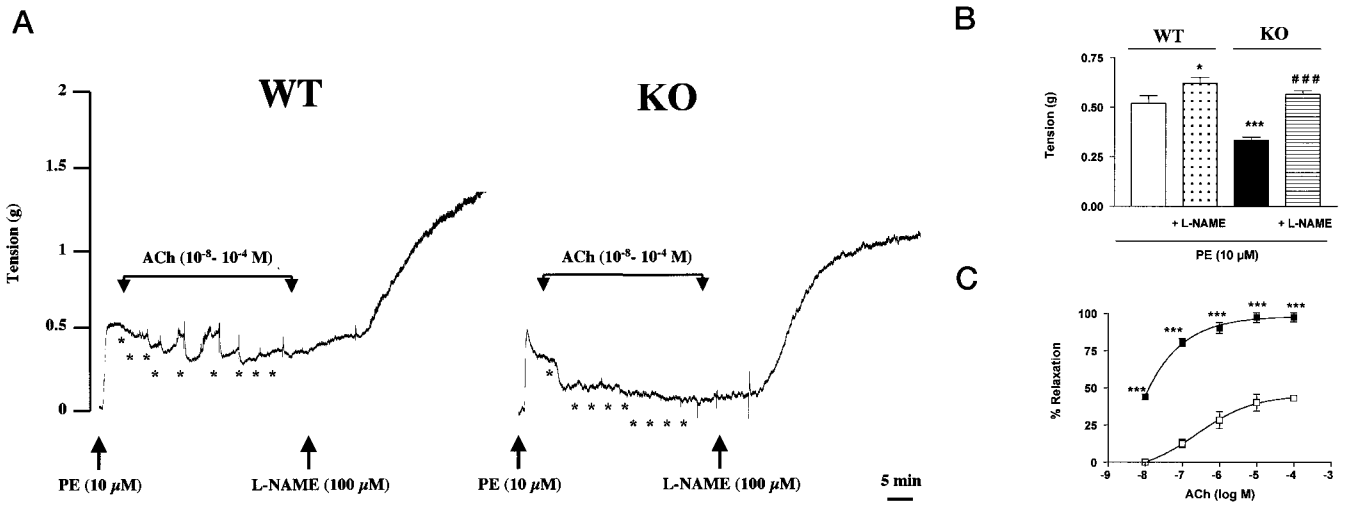

FIG. 13. **Caveolin-1-deficient mice show abnormal endothelium/NO-dependent modulation of mouse aortic contraction.** *A,* representative trace of concentration-dependent acetylcholine (10^{-8}–10^{-4} M)-induced relaxation, followed by addition of L-NAME (100 μM), which induced further contraction of the mouse aorta. Note the appearance of spontaneous oscillatory contractions present in the Ach concentration response curve in aortic rings from the wild-type mouse but largely absent from tracings obtained on aortic rings from the Cav-1 null mouse. As such, for comparative purposes, the % relaxation (see *C*) was calculated from the "steady-state" trough of relaxation observed for each Ach concentration. The *asterisks* indicate the times of addition of increasing amounts of Ach (10^{-8}, 3×10^{-8}, 10^{-7}, 3×10^{-7}, 10^{-6}, 3×10^{-6}, 10^{-5}, 3×10^{-5}, and 10^{-4} M (molar)). *B,* L-NAME (100 μM) modulation of PE-induced contraction in mouse aorta from wild-type (*WT*) and Cav-1 null (*KO*) mice. Points represent the mean ± S.E. of 5 (*KO*) and 6 (*WT*) rings from 3 mice each. *, $p < 0.05$ *versus* control WT; ***, $p < 0.0001$; ###, $p < 0.0001$ *versus* KO; two-way analysis of variance for repeated measures. Note that Cav-1 null mice showed (i) an impaired vasoconstrictor response to PE, and (ii) this impaired response could be rescued by treatment with L-NAME, a well characterized NOS inhibitor. *C,* concentration-dependent relaxation induced by acetylcholine (expressed as the log of molar concentration) in aortas pre-constricted with 10 μM phenylephrine from wild-type (*WT*; *open squares*) and Cav-1 null (*KO*; *black squares*) mice. Points represent mean ± S.E. of 5 (*KO*) or 6 (*WT*) rings from 3 mice each. ***, $p < 0.0001$ *versus* WT. Note that Ach-induced relaxation (a NO-dependent phenomenon) of the aortic rings was clearly potentiated by the loss of caveolin-1 expression.

the steady-state PE-induced contractile response after addition of L- NAME in the Cav-1 null mice was indistinguishable from that observed in the wild-type mice (Fig. 13, *A* and *B*).

In summary, we observed that Cav-1 null mice showed an impaired vasoconstrictor response to PE. This impaired response was due to increased eNOS activity as the proper vasoconstrictor response could be restored by treatment with L-NAME, a well characterized NOS inhibitor. Conversely, Ach-induced relaxation (a NO-dependent phenomenon) of the aortic rings was clearly potentiated by loss of caveolin-1 expression.

DISCUSSION

The discovery of caveolae by pioneering cell biologists in the 1950s added yet another major organelle to the cellular repertoire. Although the field remained relatively dormant for several decades, the advent of caveolar biology occurred in 1992 with the discovery of Cav-1 as the marker protein for such microdomains. It has become clear over the ensuing years that caveolar function is intimately liked to this marker protein.

In this study, we describe the generation of a new mouse model with an ablation of the gene encoding the Cav-1 protein. We show that the cells derived from these mice are deficient in caveolae, as determined ultrastructurally, thereby conclusively demonstrating that Cav-1 is required for caveolae formation in primary cells. Surprisingly, despite a lack of such prevalent and conspicuous organelles, these mice are both viable and fertile.

Cav-1 null MEFs are perturbed in several other ways, however. First, we show that Cav-2, a protein that is co-expressed, co-localizes, and hetero-oligomerizes with Cav-1 is severely affected in Cav-1 null cells. In the absence of caveolin-1, Cav-2 levels are reduced by ~95%. In addition, the remaining Cav-2 no longer targets to the plasma membrane but instead is sequestered within the Golgi complex. We further show that re-introduction of Cav-1 in these deficient cells can rescue this effect by elevating Cav-2 levels and recruiting it to the plasma membrane. Thus, the reduction of Cav-2 protein seems to be independent of transcriptional repression and is rather mediated by proteasomal degradation, as two inhibitors of the 26 S proteasome are able to partially reverse this effect. Second, we demonstrate the Cav-1 null MEFs fail to endocytose a known caveolar ligand, *i.e.* FITC-albumin, but show no defects in the uptake of FITC-transferrin, a marker for clathrin-mediated endocytosis. Importantly, transient expression of the caveolin-1 cDNA in Cav-1-deficient MEFs was sufficient to restore the uptake of FITC-albumin. Third, we show that Cav-1 null MEFs reveal a hyperproliferative phenotype. Cav-1 null MEFs are able to grow approximately 2-fold faster during the exponential phase and reach higher densities at confluence. These effects are due to an increase of ~25–30% in the S phase fraction. Furthermore, we demonstrate a reversion of this excess proliferation to wild-type levels by re-expressing Cav-1 in knockout cells. However, we do not find any evidence that the observed growth augmentation is due to a hyperactivation of the p42/44 MAP kinase cascade, a signaling pathway reported by many investigators to be intimately linked to caveolae/caveolin functioning. Furthermore, although we show that Cav-1 levels increase in higher passage cells (*i.e.* cells at or near senescence), a deficiency in Cav-1 is not sufficient to expedite immortalization in primary fibroblasts.

Caveolae are thought to form as a result of a local accumulation of cholesterol, glycosphingolipids, and caveolin-1 (8, 88, 89). Caveolin-1 can bind cholesterol *in vitro* (8); also, Cav-1 is a major protein bound to photoactivable forms of both cholesterol and glycolipids *in vivo* (88, 90). Although in this study we have demonstrated that physiological levels of Cav-1 protein are required for caveolae formation (in corroboration of previous overexpression studies), the mechanisms underlying this process remain entirely unknown. Primarily, this is due to the fact that the Cav-1 protein is not readily amenable to mutational analysis. Due to its ability to form a large oligomeric complex with itself and with Cav-2 (11, 70, 72, 91), its ability to coalesce

into even larger macrostructures (62), its binding to cholesterol and glycosphingolipids (8, 88–90), and its membrane-spanning properties, any deletion/mutation of the protein can confound an analysis of caveolae formation in numerous ways. For example, baculovirus-mediated expression of Cav-1 proteins lacking their oligomerization domain or C-terminal domains (*i.e.* Cav-1 Δ61–100 and Δ140–178) in Sf21 insect cells can induce vesicle formation albeit with sizes 10× normal caveolae. Our establishment of Cav-1-deficient cells can aid future studies in several ways. First, determinations of the composition of the plasma membrane in Cav-1-deficient cells could possibly establish whether the absence of caveolae is due to relative reductions in cholesterol/glycosphingolipid content or to simply the Cav-1 protein itself. Second, overexpression of Cav-1 mutants in these cells will establish an elegant screening strategy for *de novo* caveolae formation.

Based on the current study, the intricate dependence of Cav-2 on the presence of Cav-1 is obvious. Cav-2 is present at astonishingly lower levels (~5% of wild-type) in knockout tissues, is localized in the Golgi compartment, and is degraded by the proteasomal pathway. However, the degradation of Cav-2 is perhaps not entirely surprising. Rather elaborate mechanisms of quality surveillance have developed at various levels of the secretory pathway. Incompletely folded or assembled proteins are often sequestered at the endoplasmic reticulum where they are eventually degraded by the 26 S proteasome (reviewed in Refs. 92 and 93)). The few molecules that "escape" detection, traffic to the Golgi where they can again be detected and re-routed to the endoplasmic reticulum for degradation. Since Cav-2 cannot homo-oligomerize but rather hetero-oligomerizes with Cav-1, it is possible that in the absence of Cav-1, several critical hydrophobic regions remain exposed, thereby affecting not only folding of Cav-2 but increasing the probability of recognition by the proteasomal apparatus. To date, however, much less is known about Cav-2 function than is for Cav-1 function. Cav-2 does not contain a scaffolding domain (the primary proposed region of interaction between Cav-1 and signaling molecules) and has rarely been implicated in signal transduction processes. Although there is no overt reason to believe that its severely reduced levels in Cav-1-deficient cells can compound any phenotypic analyses, the fact remains that Cav-1 knockout mice are in effect deficient in two caveolins. The generation of Cav-2 knockout mice will ultimately resolve this issue.

Based on the growth curves of MEFs and the corresponding cell cycle analyses, we have shown in this study that a deficiency in Cav-1 leads to higher proliferation rates. This is the first direct demonstration of a relationship between Cav-1 and the cell cycle under physiological circumstances. Our results corroborate previous data showing that Cav-1 overexpression can reduce cell proliferation and/or abrogate anchorage-independent growth in several cancer cell lines (29, 31, 61). Surprisingly, we found that this proliferation is not due to a hyperactivation of the p42/44 MAP kinase cascade, a signaling pathway that had been shown in numerous ways to be reciprocally regulated by Cav-1 (28, 48, 49, 61, 81, 94).

The main difference in our study lies in the use of embryonic fibroblasts, instead of immortalized and transformed cell lines. This type of discrepancy is not unusual and necessitates the analysis of proteins in primary culture systems, such as this one. For example, the *ras* oncogene, a potent transforming agent when used in immortalized cells (95, 96), actually induces cell cycle arrest and premature senescence in MEFs (97, 98). In the same way, the mechanistic explanation of the excessive proliferation of Cav-1-deficient primary cells may depend on other signal transduction processes. Although several other pro-proliferative signaling molecules have been shown to be regulated by Cav-1, further work is required to determine more closely their physiological relevance. Analysis of these pathways in knockout *versus* wild-type MEFs will eventually shed light on the detailed mechanism for the observed hyperproliferation. In addition, although we have not noticed any spontaneous tumors in Cav-1 null mice at 9 months of age, they may have a higher susceptibility than wild-type mice to tumors induced either chemically or by breeding with other tumor-prone mice (*e.g.* the p53- or INK4a-deficient mice (79, 99)).

It should be noted that the lack of spontaneous tumor formation and the modest proliferation defect observed in the Cav-1 null setting is reminiscent of several previously described mice lacking inhibitory cell cycle proteins. For example, mice deficient in the cyclin-dependent kinase inhibitor, p21 (which functions in G_1 phase progression (100, 101) and is a major target of p53 (102)), do not develop tumors, and their MEFs display only a modest proliferative advantage over the wild-type counterparts (65). The ablation of the $p19^{INK4d}$, a member of the INK4 (inhibitor of cyclin-dependent kinase 4/6) family of proteins, also does not predispose mice to tumors or cell cycle defects (103). A deficiency of $p15^{INK4b}$ predisposes only a small percentage of mice to tumors (104). Although mice lacking p27, another important cyclin-dependent kinase inhibitor, can develop pituitary tumors, cells derived from these mice only show subtle cell cycle defects (105, 106). In many instances, the lack of an overt phenotype can be due to compensatory proteins (*i.e.* compensation derived from parallel-acting cell cycle and checkpoint control pathways). We assessed a possible up-regulation of caveolin-3, the highly homologous muscle-specific caveolin family member, in several Cav-1 null tissues, and we found it to remain unperturbed. Therefore, if there are any counter-regulatory mechanisms involved, they are independent of the caveolin gene family.

In accordance with the hyperproliferative phenotype we observed with Cav-1 null MEFs, the lung parenchyma of Cav-1 null animals appeared hypercellular with thickened alveolar septa. Quantitation of the number of nuclei per high power field using hematoxylin-eosin-stained paraffin sections revealed an ~2-fold increase in cellularity. The Ki67 "proliferation" antigen is a nuclear protein that is highly expressed in proliferating cells and is undetectable in cells in the G_0 phase of the cell cycle (83). Interestingly, Ki67 immunoreactivity was also dramatically increased in lung tissue sections from Cav-1 null mice. This is consistent with our observation that Cav-1-deficient MEFs proliferate faster and to higher saturation densities. We also found that the number of VEGF-R-positive lung endothelial cells were increased in Cav-1 null animals. These VEGF-R-positive endothelial cells were sometimes present in discrete clusters, *i.e.* reminiscent of a focus of cellular growth. Transmission electron microscopy revealed that lung endothelial cells from Cav-1 null mice lack caveolae, whereas their normal counterparts in wild-type mice showed abundant caveolae. Taken together, these findings are consistent with the idea that a lack of caveolin-1 expression and caveolae organelles can lead to hyperproliferation in certain cell types. These lung abnormalities appeared to have physical consequences, as the Cav-1-deficient mice clearly showed exercise intolerance.

Several *in vitro* studies employing recombinant expression and peptide-based analyses have strongly suggested that caveolin-1 can function as an endogenous negative regulator of eNOS, by providing tonic inhibition of eNOS enzymatic activity (85–87). Here, by using isolated mouse aortic rings, we evaluated the effect of loss of caveolin-1 expression on the vasoconstrictor actions of PE, an α_1-adrenergic receptor agonist. We observed that Cav-1 null mice showed an impaired vasocon-

strictor response to PE. This impaired response was due to increased eNOS activity as the proper vasoconstrictor response could be restored by treatment with L-NAME, a well characterized NOS inhibitor. Conversely, acetylcholine (Ach)-induced relaxation (a NO-dependent phenomenon) of the aortic rings was clearly potentiated by loss of caveolin-1 expression. These physiological observations provide strong *in vivo* evidence that caveolin-1 indeed functions as a tonic inhibitor of eNOS-mediated signal transduction.

Our current studies directly support the findings of Sessa and colleagues (107) who used a chimeric peptide containing a cellular internalization signal and the caveolin-1 scaffolding domain (CSD, residues 82–101). By using mouse aortic rings from wild-type mice, they showed that the CSD could potentiate the vasoconstrictor response to PE and that the CSD could inhibit Ach-induced relaxation of the blood vessel. The actions of the CSD could be mimicked by using the NOS inhibitor, L-NAME. In further support of the specificity of the CSD, a scrambled peptide version of the CSD had no activity in this assay system.

In summary, by using targeted disruption of the caveolin-1 gene in mice, we have shown that Cav-1 expression is required to stabilize the Cav-2 protein product, to mediate the caveolar endocytosis of specific ligands, to negatively regulate the proliferation of certain cell types, and to provide tonic inhibition of eNOS activity in endothelial cells. The availability of a viable Cav-1-deficient mouse model will allow investigators to critically evaluate the many proposed functions of the Cav-1 protein and caveolae organelles *in vivo*.

Acknowledgments—We thank Drs. David Baltimore and Anthony J. Koleske for participating in the early stages of this study. We also thank Dr. Roberto Campos-Gonzalez for donating mAbs directed against caveolin-1, caveolin-2, and caveolin-3; Dr. Tony Karnezis for help with cell cycle analysis; and Dr. Michael Cammer for help with photography.

Note Added in Proof—After this paper was published online (July 16, 2001), another report appeared online describing the generation of caveolin-1 knockout mice (August 9, 2001; Ref. 108). In accordance with our results, these authors demonstrate that loss of caveolin-1 expression prevents caveolae formation, induces a loss of caveolin-2 expression, and causes lung hypercellularity and vascular defects, as well as exercise intolerance. However, these authors did not examine the phenotypic behavior of MEFs in culture or further study the hyperproliferative phenotype. In addition, they did not examine the endocytic behavior of caveolin-1 deficient cells. Both reports (our paper and Ref. 108) conclude that the observed caveolin-1 null phenotype is consistent with the idea that caveolin-1 is a negative regulator of signal transduction and that caveolin-1 may indeed function as a tumor suppressor gene.

REFERENCES

1. Glenney, J. R., Jr. (1989) *J. Biol. Chem.* **264,** 20163–20166
2. Glenney, J. R., Jr., and Zokas, L. (1989) *J. Cell Biol.* **108,** 2401–2408
3. Rothberg, K. G., Heuser, J. E., Donzell, W. C., Ying, Y. S., Glenney, J. R., and Anderson, R. G. (1992) *Cell* **68,** 673–682
4. Yamada, E. (1955) *J. Biophys. Biochem. Cytol.* **1,** 445–458
5. Farquhar, M., and Palade, G. (1963) *J. Cell Biol.* **17,** 375–412
6. Fra, A. M., Williamson, E., Simons, K., and Parton, R. G. (1995) *Proc. Natl. Acad. Sci., U. S. A.* **92,** 8655–8659
7. Li, S., Song, K. S., Koh, S. S., Kikuchi, A., and Lisanti, M. P. (1996) *J. Biol. Chem.* **271,** 28647–28654
8. Murata, M., Peranen, J., Schreiner, R., Weiland, F., Kurzchalia, T., and Simons, K. (1995) *Proc. Natl. Acad. Sci. U. S. A.* **92,** 10339–10343
9. Scherer, P. E., Okamoto, T., Chun, M., Nishimoto, I., Lodish, H. F., and Lisanti, M. P. (1996) *Proc. Natl. Acad. Sci. U. S. A.* **93,** 131–135
10. Song, K. S., Scherer, P. E., Tang, Z.-L., Okamoto, T., Li, S., Chafel, M., Chu, C., Kohtz, D. S., and Lisanti, M. P. (1996) *J. Biol. Chem.* **271,** 15160–15165
11. Scherer, P. E., Lewis, R. Y., Volonte, D., Engelman, J. A., Galbiati, F., Couet, J., Kohtz, D. S., van Donselaar, E., Peters, P., and Lisanti, M. P. (1997) *J. Biol. Chem.* **272,** 29337–29346
12. Tang, Z.-L., Scherer, P. E., Okamoto, T., Song, K., Chu, C., Kohtz, D. S., Nishimoto, I., Lodish, H. F., and Lisanti, M. P. (1996) *J. Biol. Chem.* **271,** 2255–2261
13. Galbiati, F., Razani, B., and Lisanti, M. P. (2001) *Cell* **106,** 403–411
14. Razani, B., Schlegel, A., and Lisanti, M. P. (2000) *J. Cell Sci.* **113,** 2103–2109
15. Couet, J., Li, S., Okamoto, T., Scherer, P. S., and Lisanti, M. P. (1997) *Trends Cardiovasc. Med.* **7,** 103–110
16. Lisanti, M. P., Scherer, P., Tang, Z.-L., and Sargiacomo, M. (1994) *Trends Cell Biol.* **4,** 231–235
17. Li, S., Couet, J., and Lisanti, M. P. (1996) *J. Biol. Chem.* **271,** 29182–29190
18. Song, K. S., Li, S., Okamoto, T., Quilliam, L., Sargiacomo, M., and Lisanti, M. P. (1996) *J. Biol. Chem.* **271,** 9690–9697
19. Song, K. S., Sargiacomo, M., Galbiati, F., Parenti, M., and Lisanti, M. P. (1997) *Cell. Mol. Biol.* **43,** 293–303
20. Garcia-Cardena, G., Oh, P., Liu, J., Schnitzer, J. E., and Sessa, W. C. (1996) *Proc. Natl. Acad. Sci. U. S. A.* **93,** 6448–6453
21. Shaul, P. W., Smart, E. J., Robinson, L. J., German, Z., Yuhanna, I. S., Ying, Y., Anderson, R. G. W., and Michel, T. (1996) *J. Biol. Chem.* **271,** 6518–6522
22. Li, S., Okamoto, T., Chun, M., Sargiacomo, M., Casanova, J. E., Hansen, S. H., Nishimoto, I., and Lisanti, M. P. (1995) *J. Biol. Chem.* **270,** 15693–15701
23. Okamoto, T., Schlegel, A., Scherer, P. E., and Lisanti, M. P. (1998) *J. Biol. Chem.* **273,** 5419–5422
24. Couet, J., Sargiacomo, M., and Lisanti, M. P. (1997) *J. Biol. Chem.* **272,** 30429–30438
25. Yamamoto, M., Toya, Y., Jensen, R. A., and Ishikawa, Y. (1999) *Exp. Cell Res.* **247,** 380–388
26. Engelman, J. A., Lee, R. J., Karnezis, A., Bearss, D. J., Webster, M., Siegel, P., Muller, W. J., Windle, J. J., Pestell, R. G., and Lisanti, M. P. (1998) *J. Biol. Chem.* **273,** 20448–20455
27. Zundel, W., Swiersz, L. M., and Giaccia, A. (2000) *Mol. Cell. Biol.* **20,** 1507–1514
28. Koleske, A. J., Baltimore, D., and Lisanti, M. P. (1995) *Proc. Natl. Acad. Sci. U. S. A.* **92,** 1381–1385
29. Razani, B., Altschuler, Y., Zhu, L., Pestell, R. G., Mostov, K. E., and Lisanti, M. P. (2000) *Biochemistry* **39,** 13916–13924
30. Park, D. S., Razani, B., Lasorella, A., Schreiber-Agus, N., Pestell, R. G., Iavarone, A., and Lisanti, M. P. (2001) *Biochemistry* **40,** 3354–3362
31. Lee, S. W., Reimer, C. L., Oh, P., Campbel, L. D. B., and Schnitzer, J. E. (1998) *Oncogene* **16,** 1391–1397
32. Bender, F. C., Reymond, M. A., Bron, C., and Quest, A. (2000) *Cancer Res.* **60,** 5870–5878
33. Bagnoli, M., Tomassetti, A., Figini, M., Flati, S., Dolo, V., Canevari, S., and Miotti, S. (2000) *Oncogene* **19,** 4754–4763
34. Zhang, W., Razani, B., Altschuler, Y., Bouzahzah, B., Mostov, K. E., Pestell, R. G., and Lisanti, M. P. (2000) *J. Biol. Chem.* **275,** 20717–20725
35. Engelman, J. A., Zhang, X. L., and Lisanti, M. P. (1999) *FEBS Lett.* **448,** 221–230
36. Racine, C., Belanger, M., Hirabayashi, H., Boucher, M., Chakir, J., and Couet, J. (1999) *Biochem. Biophys. Res. Commun.* **255,** 580–586
37. Suzuki, T., Suzuki, Y., Hanada, K., Hashimoto, A., Redpath, J. L., Stanbridge, E. J., Nishijima, M., and Kitagawa, T. (1998) *J. Biochem.* (*Tokyo*) **124,** 383–388
38. Shridhar, V., Sun, Q. C., Miller, O. J., Kalemkerian, G. P., Petros, J., and Smith, D. I. (1997) *Oncogene* **15,** 2727–2733
39. Jenkins, R. B., Qian, J., Lee, H. K., Huang, H., Hirasawa, K., Bostwick, D. G., Proffitt, J., Wilber, K., Lieber, M. M., Liu, W., and Smith, D. I. (1998) *Cancer Res.* **58,** 759–766
40. Zenklusen, J. C., Thompson, J. C., Troncoso, P., Kagan, J., and Conti, C. J. (1994) *Cancer Res.* **54,** 6370–6373
41. Zenklusen, J. C., Bieche, I., Lidereau, R., and Conti, C. J. (1994) *Proc. Natl. Acad. Sci. U. S. A.* **91,** 12155–12158
42. Huang, H., Qian, C., Jenkins, R. B., and Smith, D. I. (1998) *Genes Chromosomes Cancer* **21,** 152–159
43. Zenklusen, J. C., Thompson, J. C., Klein-Szanto, A. J., and Conti, C. J. (1995) *Cancer Res.* **55,** 1347–1350
44. Zenklusen, J. C., Weitzel, J. N., Ball, H. G., and Conti, C. J. (1995) *Oncogene* **11,** 359–363
45. Koike, M., Takeuchi, S., Yokota, J., Park, S., Hatta, Y., Miller, C. W., Tsuruoka, N., and Koeffler, H. P. (1997) *Genes Chromosomes Cancer* **19,** 1–5
46. Achille, A., Biasi, M. O., Zamboni, G., Bogina, G., Magalini, A. R., Pederzoli, P., Perucho, M., and Scarpa, A. (1996) *Cancer Res.* **56,** 3808–3813
47. Engelman, J. A., Zhang, X. L., Galbiati, F., Volonte, D., Sotgia, F., Pestell, R. G., Minetti, C., Scherer, P. E., Okamoto, T., and Lisanti, M. P. (1998) *Am. J. Hum. Genet.* **63,** 1578–1587
48. Galbiati, F., Volonté, D., Engelman, J. A., Watanabe, G., Burk, R., Pestell, R., and Lisanti, M. P. (1998) *EMBO J.* **17,** 6633–6648
49. Scheel, J., Srinivasan, J., Honnert, U., Henske, A., and Kurzchalia, T. V. (1999) *Nat. Cell Biol.* **1,** 127–129
50. Hayashi, K., Matsuda, S., Machida, K., Yamamoto, T., Fukuda, Y., Nimura, Y., Hayakawa, T., and Hamaguchi, M. (2001) *Cancer Res.* **61,** 2361–2364
51. Minetti, C., Sotgia, F., Bruno, C., Scartezzini, P., Broda, P., Bado, M., Masetti, E., Mazzocco, P., Egeo, A., Donati, M. A., Volonte', D., Galbiati, F., Cordone, G., Bricarelli, F. D., Lisanti, M. P., and Zara, F. (1998) *Nat. Genet.* **18,** 365–368
52. Scherer, P. E., Tang, Z.-L., Chun, M. C., Sargiacomo, M., Lodish, H. F., and Lisanti, M. P. (1995) *J. Biol. Chem.* **270,** 16395–16401
53. Wu, H., Liu, X., and Jaenisch, R. (1994) *Proc. Natl. Acad. Sci. U. S. A.* **91,** 2819–2823
54. Wu, H., Liu, X., Jaenisch, R., and Lodish, H. F. (1995) *Cell* **83,** 59–67
55. Engelman, J. A., Zhang, X. L., Galbiati, F., and Lisanti, M. P. (1998) *FEBS Lett.* **429,** 330–336
56. Ioffe, E., Liu, Y., Bhaumik, M., Poirier, F., Factor, S. M., and Stanley, P. (1995) *Proc. Natl. Acad. Sci. U. S. A.* **92,** 7357–7361
57. Edelmann, W., Yang, K., Umar, A., Heyer, J., Lau, K., Fan, K., Liedtke, W., Cohen, P. E., Kane, M. F., Lipford, J. R., Yu, N., Crouse, G. F., Pollard, J. W., Kunkel, T., Lipkin, M., Kolodner, R., and Kucherlapati, R. (1997) *Cell* **91,** 467–477
58. Kamijo, T., Zindy, F., Roussel, M. F., Quelle, D. E., Downing, J. R., Ashmun, R. A., Grosveld, G., and Sherr, C. J. (1997) *Cell* **91,** 649–659
59. Sargiacomo, M., Sudol, M., Tang, Z.-L., and Lisanti, M. P. (1993) *J. Cell Biol.*

122, 789–807
60. Lisanti, M. P., Scherer, P. E., Vidugiriene, J., Tang, Z.-L., Hermanoski-Vosatka, A., Tu, Y.-H., Cook, R. F., and Sargiacomo, M. (1994) *J. Cell Biol.* **126,** 111–126
61. Engelman, J. A., Wycoff, C. C., Yasuhara, S., Song, K. S., Okamoto, T., and Lisanti, M. P. (1997) *J. Biol. Chem.* **272,** 16374–16381
62. Song, K. S., Tang, Z.-L., Li, S., and Lisanti, M. P. (1997) *J. Biol. Chem.* **272,** 4398–4403
63. Volonte, D., Galbiati, F., and Lisanti, M. P. (1999) *FEBS Lett.* **445,** 431–439
64. Galbiati, F., Volonte, D., Minetti, C., Chu, J. B., and Lisanti, M. P. (1999) *J. Biol. Chem.* **274,** 25632–25641
65. Deng, C., Zhang, P., Harper, J. W., Elledge, S. J., and Leder, P. (1995) *Cell* **82,** 675–684
66. LeCouter, J. E., Kablar, B., Hardy, W. R., Ying, C., Megeney, L. A., May, L. L., and Rudnicki, M. A. (1998) *Mol. Cell. Biol.* **18,** 7455–7465
67. Glenney, J. R., and Soppet, D. (1992) *Proc. Natl. Acad. Sci. U. S. A.* **89,** 10517–10521
68. Hailstones, D., Sleer, L. S., Parton, R. G., and Stanley, K. K. (1998) *J. Lipid Res.* **39,** 369–379
69. Smart, E. J., Ying, Y.-S., Donzell, W. C., and Anderson, R. G. W. (1996) *J. Biol. Chem.* **271,** 29427–29435
70. Monier, S., Parton, R. G., Vogel, F., Behlke, J., Henske, A., and Kurzchalia, T. (1995) *Mol. Biol. Cell* **6,** 911–927
71. Monier, S., Dietzen, D. J., Hastings, W. R., Lublin, D. M., and Kurzchalia, T. V. (1996) *FEBS Lett.* **388,** 143–149
72. Das, K., Lewis, R. Y., Scherer, P. E., and Lisanti, M. P. (1999) *J. Biol. Chem.* **274,** 18721–18726
73. Li, S., Galbiati, F., Volonte, D., Sargiacomo, M., Engelman, J. A., Das, K., Scherer, P. E., and Lisanti, M. P. (1998) *FEBS Lett.* **434,** 127–134
74. Mora, R., Bonilha, V. L., Marmorstein, A., Scherer, P. E., Brown, D., Lisanti, M. P., and Rodriguez-Boulan, E. (1999) *J. Biol. Chem.* **274,** 25708–25717
75. Parolini, I., Sargiacomo, M., Galbiati, F., Rizzo, G., Grignani, F., Engelman, J. A., Okamoto, T., Ikezu, T., Scherer, P. E., Mora, R., Rodriguez-Boulan, E., Peschle, C., and Lisanti, M. P. (1999) *J. Biol. Chem.* **274,** 25718–25725
76. Rock, K. L., Gramm, C., Rothstein, L., Clark, K., Stein, R., Dick, L., Hwang, D., and Goldberg, A. L. (1994) *Cell* **78,** 761–771
77. Lowe, J., Stock, D., Jap, B., Zwickl, P., Baumeister, W., and Huber, R. (1995) *Science* **268,** 533–539
78. Ghitescu, L., Fixman, A., Simionescu, M., and Simionescu, N. (1986) *J. Cell Biol.* **102,** 1304–1311
79. Serrano, M., Lee, H., Chin, L., Cordon-Cardo, C., Beach, D., and DePinho, R. A. (1996) *Cell* **85,** 27–37
80. Herrera, R. E., Sah, V. P., Williams, B. O., Makela, T. P., Weinberg, R. A., and Jacks, T. (1996) *Mol. Cell. Biol.* **16,** 2402–2407
81. Furuchi, T., and Anderson, R. G. W. (1998) *J. Biol. Chem.* **273,** 21099–21104
82. Park, W. Y., Park, J. S., Cho, K. A., Kim, D. I., Ko, Y. G., Seo, J. S., and Park, S. C. (2000) *J. Biol. Chem.* **275,** 20847–20852
83. Schluter, C., Duchrow, M., Wohlenberg, C., Becker, M. H., Key, G., Flad, H. D., and Gerdes, J. (1993) *J. Cell Biol.* **123,** 513–522
84. Gerdes, J., Li, L., Schlueter, C., Duchrow, M., Wohlenberg, C., Gerlach, C., Stahmer, I., Kloth, S., Brandt, E., and Flad, H. D. (1991) *Am. J. Pathol.* **138,** 867–873
85. Garcia-Cardena, G., Martasek, P., Siler-Masters, B. S., Skidd, P. M., Couet, J. C., Li, S., Lisanti, M. P., and Sessa, W. C. (1997) *J. Biol. Chem.* **272,** 25437–25440
86. Ju, H., Zou, R., Venema, V. J., and Venema, R. C. (1997) *J. Biol. Chem.* **272,** 18522–18525
87. Michel, J. B., Feron, O., Sacks, D., and Michel, T. (1997) *J. Biol. Chem.* **272,** 15583–15586
88. Fra, A. M., Masserini, M., Palestini, P., Sonnino, S., and Simons, K. (1995) *FEBS Lett.* **375,** 11–14
89. Li, S., Song, K. S., and Lisanti, M. P. (1996) *J. Biol. Chem.* **271,** 568–573
90. Thiele, C., Hannah, M. J., Fahrenholz, F., and Huttner, W. B. (2000) *Nat. Cell Biol.* **2,** 42–49
91. Sargiacomo, M., Scherer, P. E., Tang, Z.-L., Kubler, E., Song, K. S., Sanders, M. C., and Lisanti, M. P. (1995) *Proc. Natl. Acad. Sci. U. S. A.* **92,** 9407–9411
92. Wickner, S., Maurizi, M. R., and Gottesman, S. (1999) *Science* **286,** 1888–1893
93. Ellgaard, L., Molinari, M., and Helenius, A. (1999) *Science* **286,** 1882–1888
94. Engelman, J. A., Chu, C., Lin, A., Jo, H., Ikezu, T., Okamoto, T., Kohtz, D. S., and Lisanti, M. P. (1998) *FEBS Lett.* **428,** 205–211
95. Shimizu, K., Goldfarb, M., Suard, Y., Perucho, M., Li, Y., Kamata, T., Feramisco, J., Stavnezer, E., Fogh, J., and Wigler, M. H. (1983) *Proc. Natl. Acad. Sci. U. S. A.* **80,** 2112–2116
96. Newbold, R. F., and Overell, R. W. (1983) *Nature* **304,** 648–651
97. Serrano, M., Lin, A. W., McCurrach, M. E., Beach, D., and Lowe, S. W. (1997) *Cell* **88,** 593–602
98. Lin, A. W., Barradas, M., Stone, J. C., van Aelst, L., Serrano, M., and Lowe, S. W. (1998) *Genes Dev.* **12,** 3008–3019
99. Sah, V. P., Attardi, L. D., Mulligan, G. J., Williams, B. O., Bronson, R. T., and Jacks, T. (1995) *Nat. Genet.* **10,** 175–180
100. Harper, J., Adam, G., Wei, N., Keyomarsi, K., and Elledge, S. (1993) *Cell* **75,** 805–816
101. Harper, J. W., Elledge, S. J., Keyomarsi, K., Dynlacht, B., Tsai, L. H., Zhang, P., Dobrowolski, S., Bai, C., Connell-Crowley, L., and Swindell, E. (1995) *Mol. Biol. Cell* **6,** 387–400
102. el-Deiry, W. S., Tokino, T., Velculescu, V. E., Levy, D. B., Parsons, R., Trent, J. M., Lin, D., Mercer, W. E., Kinzler, K. W., and Vogelstein, B. (1993) *Cell* **75,** 817–825
103. Zindy, F., van Deursen, J., Grosveld, G., Sherr, C. J., and Roussel, M. F. (2000) *Mol. Cell. Biol.* **20,** 372–378
104. Latres, E., Malumbres, M., Sotillo, R., Martin, J., Ortega, S., Martin-Caballero, J., Flores, J. M., Cordon-Cardo, C., and Barbacid, M. (2000) *EMBO J.* **19,** 3496–3506
105. Fero, M. L., Rivkin, M., Tasch, M., Porter, P., Carow, C. E., Firpo, E., Polyak, K., Tsai, L. H., Broudy, V., Perlmutter, R. M., Kaushansky, K., and Roberts, J. M. (1996) *Cell* **85,** 733–744
106. Coats, S., Whyte, P., Fero, M. L., Lacy, S., Chung, G., Randel, E., Firpo, E., and Roberts, J. M. (1999) *Curr. Biol.* **9,** 163–173
107. Bucci, M., Gratton, J. P., Rudic, R. D., Acevedo, L., Roviezzo, F., Cirino, G., and Sessa, W. C. (2000) *Nat. Med.* **6,** 1362–1367
108. Drab, M., Verkade, P., Elger, M., Kasper, M., Lohn, M., Lauterbach, B., Menne, J., Lindschau, C., Mende, F., Luft, F. C., Schedl, A., Haller, H., and Kurzchalia, T. V. (2001) *Science*, in press, Published Online August 9, 2001, 10.1126/science.1062688

Caveolin-1 Null Mice Are Viable but Show Evidence of Hyperproliferative and Vascular Abnormalities

Babak Razani, Jeffery A. Engelman, Xiao Bo Wang, William Schubert, Xiao Lan Zhang, Carolyn B. Marks, Frank Macaluso, Robert G. Russell, Maomi Li, Richard G. Pestell, Dolores Di Vizio, Harry Hou, Jr., Burkhard Kneitz, Guy Lagaud, George J. Christ, Winfried Edelmann and Michael P. Lisanti

J. Biol. Chem. 2001, 276:38121-38138.
originally published online October 5, 2001
